NATIONAL ADVISORY COMMITTEE FOR AERONAUTICS

TECHNICAL NOTE 3600

CORRELATION OF CRIPPLING STRENGTH OF PLATE STRUCTURES WITH MATERIAL PROPERTIES

By Roger A. Anderson and Melvin S. Anderson

Langley Aeronautical Laboratory
Langley Field, Va.

Washington
January 1956

NATIONAL ADVISORY COMMITTEE FOR AERONAUTICS

TECHNICAL NOTE 3600

CORRELATION OF CRIPPLING STRENGTH OF PLATE STRUCTURES WITH MATERIAL PROPERTIES

By Roger A. Anderson and Melvin S. Anderson

SUMMARY

A correlation approach to the crippling-strength analysis of plate structures in new materials and at elevated temperatures is presented. Appropriately defined crippling-strength moduli and correlation procedures are given for predicting the effect of a change in material properties on the strength of a structure. The strength moduli are readily calculated from the effective compressive stress-strain curve for the structural material. The correlation procedures are applicable to multi-plate-element components and the accuracy is illustrated with available experimental data obtained in various materials and under different temperature conditions.

INTRODUCTION

A problem which is confronting the aircraft structural designer with increasing frequency is the prediction of the effect of large changes in material properties on the strength of airframe components. These changes may be due to the effects of heat on present airframe materials or may arise because of design changes to more heat-resistant materials. If the accumulated strength data at room temperature on components made of aluminum alloy are to be extended to other materials and temperature conditions, accurate procedures for correlating structural strength with material properties are required.

Whereas the ultimate tensile strength of materials is a useful guide for correlating the static strength of components loaded in tension, no single physical property of materials serves this purpose for components loaded primarily in compression. With relatively simple components, such as columns and heavily loaded plates, the buckling stress can be used as a criterion for failure, in which cases correlation among materials is readily determined from buckling moduli computed from the shape of material compressive stress-strain curves. Multi-plate-element components and stiffened plates, however, usually possess a maximum compressive strength, or crippling strength, which is greater than the stress at which some form of local buckling takes place. For these cases, various empirically

determined parameters have been proposed to effect correlation with material properties. Those most commonly used take into account the height of a material compressive stress-strain curve, as measured by a defined yield stress, in addition to either the slope of the curve (ref. 1) or a quantity such as the buckling stress (refs. 2 and 3) which is a function of the slope. The relative weight given to the height and slope of the material stress-strain curve, however, differs markedly in the parameters of references 1 to 3. This variance appears to be a consequence of differences in the material and geometry of the test specimens used to obtain the data analysed in those investigations. In addition, little published information is available to guide an application of these parameters to more complex fabricated structural components.

More recently, maximum strength analyses of stiffener sections (refs. 4 and 5), multiweb beams (refs. 6 and 7) and stiffened panels (ref. 8) have become available which clarify the respective roles which material properties and structural arrangement of the material play in determining the crippling strength of these components. As a result, for a number of complex structures, it is possible to determine a suitable material-properties parameter and to correlate failing strengths with changes in material without resorting to a complete strength analysis. The practical possibilities and limitations of this correlation approach are examined in the present paper. Crippling stresses for flat plates, multiweb beams, skin-stringer panels, and other structural components made of materials encompassing a wide variation in properties are compared with the material correlation parameter applicable to the mode of failure of the particular component. Available data from short-time strength tests at elevated temperatures are included in the comparisons. Based on these comparisons, procedures for correlating crippling strength of multi-plate-element structures with changes in material properties are recommended.

SYMBOLS

A_p	cross-sectional area of plate element, $in.^2$
b	width of plate, in.
b_o	width of attachment flange between rivet line and web plane, in.
E	Young's modulus for material, ksi
E_t	tangent modulus for material at given stress, ksi
E_s	secant modulus for material at given stress, ksi

E_s'	secant modulus associated with stress at which $E_t = (1 - m)E_s$; for larger stresses, it is equal to E_s, ksi
f, f_1, f_2	functional notation
K	nondimensional buckling-stress coefficient, $\frac{\sigma_{cr}}{\eta E}\left(\frac{b}{t}\right)^2$
m	ratio of initial slope, after elastic buckling, of curve of average stress plotted against unit shortening to slope of material stress-strain curve
M	bending moment, in-lb
n, p	integers
R	ratio of test value of crippling stress to value calculated for failure in local buckling mode
S	section modulus for beam, $in.^3$
t	thickness of plate, in.
σ	general notation for stress, ksi
$\bar{\sigma}$	average stress over cross section, ksi
σ_{cr}	buckling stress, ksi
σ_{cy}	0.2-percent-offset compressive-yield stress for material, ksi
σ_e	stress corresponding to unit shortening ϵ_e, ksi
$\bar{\sigma}_f$	maximum average or crippling stress, ksi
$\bar{\sigma}_p$	average stress for plate element at failure, ksi
σ_2	stress at which $E_t = \frac{1}{2}E_s$, ksi
σ_3	stress at which $E_t = \frac{1}{3}E_s$, ksi
ϵ	general notation for strain

ϵ_{cr} strain at which buckling initiates

ϵ_e average unit shortening or edge strain in a plate

ϵ_f average unit shortening at maximum load

ϵ_2 strain associated with σ_2

ϵ_3 strain associated with σ_3

η nondimensional plasticity correction factor

INFLUENCE OF MATERIAL PROPERTIES ON PLATE COMPRESSIVE STRENGTH

The determination of allowable compressive stresses of rectangular-plate elements is a primary consideration in aircraft structural design. Plates can be classified according to whether one or two of the unloaded edges are supported against deflection. Flat plates of the latter class are considered in this section. Inasmuch as the strength analysis differs for plates that fail at the buckling stress and those that exhibit a post-buckling strength, the presentation that follows is subdivided accordingly.

Plates That Fail at the Buckling Stress

When the stresses to be transmitted are high or the plate boundaries are flexibly supported, the maximum stress is often adequately represented by the equation for buckling

$$\frac{\sigma_{cr}}{\eta E} = K\left(\frac{t}{b}\right)^2 \qquad (1)$$

When written in this form, the value of the left-hand side of the equation may be considered a constant for a given plate geometry and σ_{cr} is essentially dependent only upon the properties of the plate material. Although theoretical work has shown that the plasticity correction factor η may be influenced to some extent by the plate-geometry and edge-restraint conditions, a consideration of these differences is usually not warranted in a buckling-stress analysis of the typical edge-supported plate encountered in fabricated aircraft structures.

An expression for η in fairly common use and one that correlates experimental buckling stresses obtained in many different materials is

$$\eta = \sqrt{\frac{E_t}{E}} \tag{2}$$

where η is computed from the average of the material compressive properties over the cross section of the test structure. For plate structures of identical geometry then, the value of $\sigma_{cr}/\eta E$ can be considered a constant, and a value of σ_{cr} determined from a test in a reference material (material 1) is sufficient to define σ_{cr} for the plate structure in any other material (material 2) provided that the variation of the buckling modulus ηE with stress is known for the materials. A convenient correlation procedure based on the constancy of $\sigma/\eta E$ for plates of constant geometry is illustrated in figure 1. The curves for the variation of σ with $\sigma/\eta E$ are computed from the compressive stress-strain curves for the desired materials and the buckling stresses of plates of these materials are correlated in the manner indicated. The inherent accuracy of the procedure is good when the diagram is entered with a known stress in the more elastic material, as shown in figure 1. Comparable accuracy cannot be expected when the known buckling stress is in the inelastic range of the lower strength material because of the relatively larger variations in $\sigma/\eta E$ associated with small errors in stress.

Plates With Post-Buckling Strength

Equations similar to equation (1) have been proposed for the maximum stress of plates which carry additional load after buckling. In these equations a parameter frequently used to represent the influence of material is the quantity $(E\sigma_{cy})^{1/2}$, which was developed in reference 1 and applied to correlating the strength of plates of various materials when tested in V-groove edge fixtures. The plates had relatively high values of width-thickness ratio b/t. The same parameter appears in crippling-strength formulas for stiffener sections (refs. 4 and 9). A parameter of this type incorporates the prominent features of a materials compressive stress-strain curve, that is, initial slope and a stress level (height) at which pronounced plastic yielding occurs for most materials. With respect to a compressed plate, the slope and height of the material stress-strain curve can be thought of, respectively, as a measure of the relative stiffness of materials in resisting buckling distortion and a measure of the maximum stress that can be attained in the most highly strained portions of the plate.

In studies of the buckling and crippling stresses of aluminum- and magnesium-alloy plates in the form of H, Z, and C sections (refs. 2 and 3), strength formulas are given which contain parameters of the type $(\sigma_{cr}\sigma_{cy}^{n-1})^{1/n}$. Values of n equal to 5 and 4 were assigned in references 2 and 3, respectively. For a plate of a given geometry, the value of σ_{cr}, in effect, is a measure of the slope of the stress-strain curve for the plate material, and a material parameter $(\eta E\sigma_{cy}^{n-1})^{1/n}$ can be separated from the quantities describing the section geometry. For n equal to either 4 or 5, this parameter is in conflict with the parameter $(E\sigma_{cy})^{1/2}$ proposed by other investigators.

In order to determine which of the foregoing parameters or modifications of them is likely to give the best overall representation of the influence of material on the compressive strength of edge-supported plates, a series of flat plates supported in V-groove edge fixtures were tested to failure as part of the present investigation. In tests of this type no forming operations are performed in manufacturing the specimen and material stress-strain coupons cut from the sheet material adjacent to the plate specimens should be representative of the plate material. The materials selected covered a wide range in E, σ_{cy}, and shape of compressive stress-strain curve and the plates tested had width-thickness ratios representative of thick-skin construction. Details of this test investigation are given in appendix A.

Compressive stress-strain curves representative of the materials in the plates tested are given in figure 2. Included is a stress-strain curve for the 2014-T6 square tubes tested in reference 10. (The compressive strength of plates forming the walls of a square tube are in apparent agreement with the strength of plates in V-groove edge fixtures.) A different treatment is indicated in figure 2(f) for an 18-8-$\frac{3}{4}$H stainless steel (type 301). "Effective stress-strain" curves were constructed for this anisotropic material which are explained in appendix B. In addition to values of E and σ_{cy}, a stress and strain (denoted σ_2 and ϵ_2) at which the tangent modulus to the curves is equal to one-half the secant modulus are noted on the stress-strain curves.

Material correlation parameters computed from the stress-strain data of figure 2 are compared with the test crippling stresses for the plates in figures 3 and 4. Figure 3 compares the test data with the parameters $(E\sigma_{cy})^{1/2}$ and $(\eta E\sigma_{cy}^{3})^{1/4}$ discussed previously. In these plots, correlation would be indicated if the data for plates of all materials lay on a single curve. Although the data for the various materials intermingle, an appreciable scatter band exists.

In an attempt to reduce the scatter band, simple modifications to the material parameters were investigated. An analysis of the data revealed that the scatter band associated with $(E\sigma_{cy})^{1/2}$ would be decreased if a reduced value of E were used for the plates of smaller b/t the crippling stresses of which occur in the inelastic stress range. A convenient correction of this type involves using the value of the secant modulus E_s at the crippling stress in place of the constant value E. A plot of the data against $(E_s\sigma_{cy})^{1/2}$ is shown in figure 4(a) and an improvement over figure 3 is obtained. The scatter which remains appears to be associated with the differences in shape of stress-strain curves in the inelastic range.

In order to account for the effect of differences in shape, material parameters can be defined which are sensitive to the rate of change of slope of material stress-strain curves. One such parameter is the maximum value of the quantity $(E_s\sigma)^{1/2}$. The relationship of this quantity to $(E\sigma_{cy})^{1/2}$ for the plate materials is shown in table I. The ratio of the two quantities for some of the materials is constant whereas for other materials significant differences occur.

The maximum value of $(E_s\sigma)^{1/2}$ is shown in appendix C to occur at the stress and strain at which the tangent modulus has become equal to one-half the secant modulus. The corresponding material correlation parameter $(E'\sigma_2)^{1/2}$ characterizes a material by a stress level σ_2 near the knee of its stress-strain curve where its stiffness is changing rapidly and by a secant slope E' passing through the point σ_2, ϵ_2. As with the parameter $(E\sigma_{cy})^{1/2}$, best correlation with data at high stress levels is obtained when $(E'\sigma_2)^{1/2}$ is modified so that it varies with stress. This modification is accomplished by defining a modified parameter $(E_s'\sigma_2)^{1/2}$ which is equal to $(E'\sigma_2)^{1/2}$ for stresses less than σ_2 but in which the value of E_s' is equal to the conventional secant modulus for stresses larger than σ_2. A comparison of the data using the parameter $(E_s'\sigma_2)^{1/2}$ is shown in figure 4(b).

The comparisons presented in figures 3 and 4 indicate that either of the parameters $(E_s\sigma_{cy})^{1/2}$ and $(E_s'\sigma_2)^{1/2}$ gives a better correlation of the data than the parameters $(E\sigma_{cy})^{1/2}$ and $(\eta E\sigma_{cy}^3)^{1/4}$, the best

correlation being obtained with $(E_s'\sigma_2)^{1/2}$. Suitable maximum-strength formulas for plates can therefore be written in the form

$$\frac{\bar{\sigma}_f}{(E_s\sigma_{cy})^{1/2}} = f_1\left(\frac{t}{b}\right) \tag{3a}$$

$$\frac{\bar{\sigma}_f}{(E_s'\sigma_2)^{1/2}} = f_2\left(\frac{t}{b}\right) \tag{3b}$$

A good representation of the data below a b/t of 45 is provided by the simple equations in figure 4.

For the purpose of a crippling-strength calculation, the material parameters in equations (3) adequately describe the influence of material on the compressive strength of plates with supported edges. Such parameters will therefore be referred to in this paper as crippling-strength moduli, or more briefly as strength moduli, the form of which depend upon the structure and its mode of failure. The plate-strength-correlation procedure with these moduli is analogous to that previously described for plate buckling and is illustrated in figure 5.

In the remainder of the paper the strength moduli applicable to plates tested in V-groove edge fixtures are assumed to apply to all edge-supported plates. Suitable correlation procedures are developed when the plates are part of a fabricated structure. Because the parameter $(E_s\sigma_{cy})^{1/2}$ involves material properties that are more generally available than the properties in $(E_s'\sigma_2)^{1/2}$, particularly at elevated temperatures, the crippling-strength comparisons involving plate elements with supported edges are made by using $(E_s\sigma_{cy})^{1/2}$ as the strength modulus.

INFLUENCE OF MATERIAL PROPERTIES ON STIFFENER CRIPPLING STRENGTH

The usual engineering method for calculating the crippling strength of stiffeners (column bending excluded as a failure mode) is to sum the loads carried by web and flange plate elements in the cross section.

Variations of this method are exemplified in references 4, 5, and 11. The success of this approach is dependent upon the accuracy of the crippling curves which are used to define the maximum compressive stresses for the individual plate elements. An alternate approach is to relate the crippling stress of the entire cross section to its local buckling stress and the material yield stress as is done in references 2 and 3. This approach lacks the generality of the first approach, however, inasmuch as the most suitable relationship between $\bar{\sigma}_f$, σ_{cr}, and σ_{cy} varies with changes in cross section.

In a crippling-strength study (ref. 5) of both extruded and formed cross sections based upon the first approach, good correlation of the strength of plates with one edge supported and one edge free (flanges) with changes in material was found with equations of the form

$$\frac{\bar{\sigma}_f}{(E_s'\sigma_3^2)^{1/3}} = f\left(\frac{b}{t}\right) \tag{4}$$

One function of b/t was obtained when a single flange joined a web plate (as in a Z-section) and another function of b/t was obtained when two flanges joined a web plate (as in an I-section). The material parameter $(E_s'\sigma_3^2)^{1/3}$, used to correlate flange strength with changes in material, is related to that used in equation (3(b)) for plates with two edges supported. In appendix B it is shown that the reference stress level σ_3 for a material corresponds to the stress at which the tangent modulus is equal to one-third the secant modulus. The value of E_s' is equal to the secant modulus at σ_3 with the provision that, at average values of flange stress greater than σ_3, E_s' is defined as E_s.

An approximation of the parameter $(E_s'\sigma_3^2)^{1/3}$ which involves readily available material properties is the quantity $(E_s\sigma_{cy}^2)^{1/3}$. This strength modulus implies that flange strength is more a function of material yield stress than material elastic modulus. The test data of reference 5 bear this out as shown by comparison of the correlation accuracy in figure 6 where the data have been plotted by using $(E_s\sigma_{cy}^2)^{1/3}$ and $(E_s\sigma_{cy})^{1/2}$ as strength moduli. The data for extruded and formed cross

sections are brought into agreement when the strength moduli are computed from effective stress-strain curves which take into account high-strength material in the corners of formed sections. These curves are explained in appendix C.

When only the geometry of an extruded or formed cross section composed of essentially flat-plate elements is known and the crippling strength in any material is desired, a strength-analysis method such as that of reference 5 is required. If the crippling stress for a stiffener section is known from a test in a reference material, however, its strength in another material may often be obtained more accurately by the correlation approach. An indication of the accuracy obtainable is shown by the comparison in figure 7 of crippling-stress data for a family of Z-sections of a number of materials. The data correspond to Z-sections having a constant ratio of flange width to web width (0.6) and are therefore plotted against the width-thickness ratio of a reference plate element (web), the primary geometrical variable for the data. The strength modulus used is that appropriate to a plate with supported edges and was computed from the effective stress-strain curves for the section. (See appendix B.)

For sections containing a high proportion of flange area, a strength correlation based on the constancy of $\sigma/(E_s\sigma_{cy}^2)^{1/3}$ for sections of constant geometry might be expected to give the best results. In reference 12 the crippling strength of H-sections of extruded 7075-T6 aluminum alloy were obtained at room and elevated temperatures. These data are plotted in figure 8. The predicted curves are based on the values of $\sigma/(E_s\sigma_{cy}^2)^{1/3}$ obtained in the room-temperature tests of the sections and the variation of $(E_s\sigma_{cy}^2)^{1/3}$ with temperature was calculated from the material stress-strain data given in reference 12.

INFLUENCE OF MATERIAL ON CRIPPLING STRENGTH OF STIFFENED PLATES

The compression panel of a box beam is treated in this section as a stiffened plate for which a crippling stress can be defined. For conventional rib-stringer-skin construction, this stress is defined as the upper-limit failure stress obtained when column failure is prevented by a close rib spacing. For multiweb-type structure, the crippling strength is the maximum average stress obtained in the skin- and web-attachment members under a bending moment when failure of the webs under crushing loads is not permitted. With these restrictions, a panel crippling-strength analysis is concerned principally with the geometry of the plate

elements in the cross section, the relative stiffness of the joints between them, and material properties. Even though the first two of these variables are held constant when the influence of a material change is to be determined, various modes of local failure must still be taken into account in a strength-correlation procedure. Unforeseen failure mode changes can occur when large changes in material properties are made. The nature of this problem is discussed next and the procedures for dealing with it are given in a following section.

Effect of Material Properties on Local Failure Mode

In order to illustrate the effect of material changes on the stress and mode of local failure of a stiffened plate, figure 9 has been prepared. Figure 9(a) illustrates the manner in which the crippling strength of a stiffened plate of constant geometry can vary with yield stress when the elastic modulus of the material is held constant. The crippling strength has been computed by considering three of the possible modes of local failure. The curve labeled "failure in the local buckling mode" corresponds to a failure stress computed from the area weighted average of the crippling stresses for the individual plate elements in the panel cross section. The assumption made in this calculation is that the maximum load carried by each plate element is reached at the same unit shortening and thus the loads are additive. If the average stresses achieved in the plate elements are assumed to approximate those given in figures 4(a) and 7, correlation of the stresses with changes in material properties can be effected by the strength modulus employed in those figures. Correspondingly, the local crippling strength of the panel is shown in figure 9(a) to increase as the square root of the increase in σ_{cy}. (The panel failing stress is assumed to not exceed σ_{cy} for a material; thus, as σ_{cy} decreases, the panel failing stress approaches σ_{cy} as an upper limit.) This type of performance can be expected if the stiffening members are an integral part of the sheet, as in an extruded panel.

When stiffening members have attachment flanges which are riveted to the sheet, a maximum compressive load can also be calculated at which the sheet buckles in a short wave length without longitudinal nodes along the stiffeners. The behavior is that of a plate column elastically restrained against displacement by the stiffeners attachment flanges and has been variously described as "forced crippling" (of the stringers) in reference 13 and as "wrinkling" (of the sheet) in reference 14. The first term is probably more descriptive of the action for panel proportions in which this mode of failure follows buckling of the sheet in the local mode whereas the second term appears more descriptive when buckling as well as failure occur without longitudinal nodes in the sheet.

An extensive study of the behavior of stiffened plates which fail by wrinkling has been made in references 6 and 8 and a criterion for failure is given which is of the form

$$\frac{\bar{\sigma}_f}{\eta E} = f(\text{panel geometry, attachment-flange design}) \qquad (5)$$

The influence of material on the stress for failure is represented by a buckling modulus ηE because of the close correlation between complete panel failure and the occurrence of sheet wrinkling with its attendant loss of "effective width." The wrinkling-strength curve for the panel of figure 9(a) is therefore shown to level off at a constant stress when σ_{cy} is large enough that the calculated failure stress is in the material elastic range. The magnitude of this stress for a particular panel is determined by the value of E, the panel geometry, and the stiffness of the attachment between stiffeners and sheet. When σ_{cy} is decreased, the transition from this elastic value of failure stress to failure at the material yield strength is determined by the variation of η with stress. Test data indicate that the expression for η given by equation (2) is applicable.

Analysis of the data of reference 15 reveals that riveted panels of proportions which buckle in the local mode will change from failure in the local-buckling mode to a failure that is initiated by wrinkling instability of the sheet when the ratio of σ_{cy} to E is sufficiently increased. This action is typical of most panel proportions and figure 9 has been drawn accordingly. (With an inadequate riveted attachment, wrinkling can be the lowest mode of failure at any ratio of yield stress to modulus.) In the transition region, the failure stress for some panel proportions may be somewhat less than the stresses calculated for either of the "pure" modes. These stresses are indicated by an interaction curve (dashed) in figure 9 for which no convenient material correlation parameter has as yet been found.

When panels susceptible to wrinkling failure are made of materials having very high ratios of yield stress to modulus, the maximum panel load may approach the crippling load for the stiffeners alone. The stiffener-strength curve may be assumed to represent a lower limit to a panel crippling strength and is thus shown in figure 9(a) to govern at a high value of yield stress.

When yield stress is held constant and material elastic modulus is treated as a variable, the variation of panel strength when the same three modes of local failure are considered is illustrated in figure 9(b). A comparative study of the (a) and (b) parts of figure 9 reveals a consistent

pattern of failure-mode change as material properties change. They show that a fabricated stiffened plate which fails in the local buckling mode when made of a material with a relatively low value of σ_{cy}/E, for example 2024-ST aluminum alloy, may interact with or fail in the wrinkling mode when made of a material with a higher value of σ_{cy}/E, such as 7075-ST aluminum alloy, and may only develop the strength of the stiffeners in a material such as some of the titanium alloys which have relatively high values of σ_{cy}/E. With this complex behavior, the strength modulus associated with the mode of failure (observed in a test or assumed in a calculation) in a reference material may not be applicable for predicting the effect of a large change in material properties. An added complication with existing test data on crippling strength is that the mode of local failure involved is usually unreported.

In order to cope with these problems, a practical procedure for predicting the effect of a change in material properties must start with the assumption that only the commonly reported information for a stiffened plate is available; that is, the crippling stress, material properties, and dimensions of the cross section. Although an accurate value of a key dimension, the offset of the rivet lines from the web plane of riveted-on stiffeners, is generally missing, the probable mode of failure of the panel in the reference material usually can be deduced from the available information, as explained in the next section. Recommendations formulated from consideration of figure 9 can then be made which take into account the possibility of a failure mode change as material properties are varied.

Correlation Procedure

A study of the crippling strength of the longitudinally stiffened compression panels reported in references 16 to 19 reveals that the probable mode of failure of a given panel can be correlated with the value of a coefficient R defined by

$$R = \frac{\bar{\sigma}_f \sum_p A_p}{\sum_p A_p \bar{\sigma}_p} \tag{6}$$

The stresses $\bar{\sigma}_p$ represent the crippling stresses of the component plate elements of the panel cross section as defined by the crippling curves of this paper; the areas A_p are the individual areas of the plate elements. Hence R is the ratio of test crippling stress to a calculated stress for failure in the local buckling mode.

Discounting results for panels tested flat-ended at a length less than the stringer spacing, the value of R for strongly riveted panels with extruded stringers (near integral construction) was found to lie consistently between the limits 0.95 to 1.05. These values of R are assumed to correspond to failure stresses associated with the local buckling mode of failure. Larger values of R were found for panels tested at a length less than the stringer spacing and which failed in the local buckling mode. The high crippling stresses are attributed to the constrained buckling distortion of the sheet which occurs under those test conditions. Panels with values of R less than about 0.95 had riveted-attachment-flange designs and width-thickness ratios of the sheet and stringers so that a reduction in failing stress due to wrinkling behavior would be predicted by the theory of reference 8. Therefore, in the present prccedure, test stresses with an R-value less than 0.95 are assumed to be either the result of wrinkling instability or interaction with it. The panel is further assumed to possess a potential stress for failure in the local buckling mode equal to σ_f/R. (For panels of unusual proportions, a low value of R can also correspond to a panel stress in which only the crippling strength of the stiffeners is developed. Such a test result is readily recognizable when the calculation for R is made. The effect of material property changes on panels which develop this low proportion of their potential strength is difficult to predict and, moreover, should not be of practical interest. The correlation procedure which follows is therefore not formulated to cover this case.)

The correlation procedure for stiffened plates is handled conveniently if subdivided according to the R-value for the test stress in the reference material and according to whether the material change corresponds to an increase or a decrease in the ratio σ_{cy}/E. The recommendations for the four cases which result from this subdivision are based on figure 9 and are outlined below.

Case I: R essentially unity; σ_{cy}/E decreasing.- A panel which fails in the local buckling mode in a reference material (material 1) can be assumed to fail in the same mode in a new material (material 2) if the ratio σ_{cy}/E is either constant or decreasing. The predicted panel stress in material 2 can therefore be obtained by correlating the individual crippling stresses of the stiffener and sheet elements and weighting these stresses according to area. The correlation procedure for the sheet is illustrated in figure 5. The same procedure is followed for the stiffeners with the assumption that the value of either $\sigma/(E_s\sigma_{cy})^{1/2}$ or $\sigma/(E_s\sigma_{cy}^2)^{1/3}$ for the stiffener is independent of material, as is discussed in the section on stiffener crippling strength. A further simplification is possible if the panel is proportioned so that the crippling stresses for the sheet and stringers are not too different and their material properties are essentially

the same. A strength correlation based on the constancy of $\sigma/(E_s\sigma_{cy})^{1/2}$ for the whole cross section can then be made by using an average variation of $(E_s\sigma_{cy})^{1/2}$ with stress for the material over the entire cross section.

Case II: R essentially unity; σ_{cy}/E increasing.- If the change in material properties is such that the ratio σ_{cy}/E is increasing, the possibility exists that failure of the panel in material 2 may be influenced by wrinkling behavior and the failure stress will be less than that associated with failure in the local buckling mode. The procedure outlined in case I should therefore be used with caution when the effect of a substantial increase in σ_{cy}/E is to be determined for a panel with riveted-on stiffening members. For panels with integral stiffening, the procedure for case I should be applicable.

Case III: R less than 0.95; σ_{cy}/E decreasing.- A panel influenced by wrinkling behavior in material 1 may fail in either the wrinkling mode or local buckling mode if the ratio σ_{cy}/E is decreased. Inasmuch as the stresses for failure in both of these modes ($\bar{\sigma}_f$ and $\bar{\sigma}_f/R$) are assumed to be known in material 1, the stresses for failure in both modes can be predicted in material 2. The lower of these predicted stresses is assumed to govern.

In order to predict the change in strength of a panel in the wrinkling mode, the procedure indicated in figure 1 is applicable. The figure is entered with $\bar{\sigma}_f$ in material 1 and the corresponding stress for material 2 is found at a constant value of $\sigma/\eta E$. The variation of ηE with stress for the two materials should be computed from the average material properties over the panel cross section. The effect of the material change on the stress for failure in the local buckling mode is determined by the procedure previously outlined for case I. Because the actual failure stress for the panel in material 2 could lie in the transition region shown by dashed curves in figure 9, the above correlation procedure can be anticipated to be slightly unconservative under certain circumstances.

Case IV: R less than 0.95; σ_{cy}/E increasing.- If the ratio σ_{cy}/E is larger for material 2 than for material 1, a further reduction in failure stress from the value for the local buckling mode can be anticipated in material 2. The failure stress will be bracketed by the stresses predicted by the procedure for case III. A conservative prediction therefore can always be obtained if the panel is assumed to fail at a constant value of $\sigma/\eta E$. Test data show that the inherent conservatism of this assumption is reduced as the value of R for the panel in the reference material becomes less.

Experimental Verification

Verification of the recommended correlation procedures for stiffened plates has been made with the available data for nominally identical specimens tested in various materials. These data consist principally of a series of Z-stringer compression panels tested in nine different materials (ref. 15) and miscellaneous tests on stiffened panels and multiweb beams at room and elevated temperatures. In order to illustrate the correlation accuracy obtainable under differing circumstances, comparisons with some of these test data are presented in tables II to V and in figure 10.

The test data in tables II, III, and IV are from reference 15 and are representative of three typical types of behavior in longitudinally stiffened panels. The panel in table II has relatively large width-thickness ratios of the plate elements and the riveting is adequate to develop an R-value of essentially unity in 7075-T6 aluminum alloy. This material has the highest ratio of σ_{cy} to E of the materials tested in reference 15 and its material properties are also known with the greatest certainty. For these reasons the predicted failing strength of the panel in the other materials is based on the test failing strength in 7075-T6. The procedure for case I was applied by using effective stress-strain curves for the materials based on the average longitudinal and formed-corner properties for the materials as given in reference 15. The predicted failing strengths generally are in as good agreement with the test results as would be anticipated from the deviation of the given minimum and maximum material properties from the average. The largest error is associated with the 18-8-$\frac{3}{4}$H steel, the panels of which were fabricated with an offset of the rivet line on the attachment flanges of the stiffeners 10 percent larger than the average of the otherwise nominally identical panels in the other materials. The effect of this difference is to reduce the test crippling strength of the panels of the 18-8-$\frac{3}{4}$H material relative to the panels of the other materials.

The panel in table III has one-half the width-thickness ratio of the plate elements of the previous panel and the same rivet and attachment flange design. This combination, although adequate to produce initial buckling in the local mode, is not adequate to obtain a failing stress in 7075-T6 aluminum alloy corresponding to failure in the local buckling mode, as evidenced by an R-value of 0.91 for the panel. This R-value is interpreted as an indication that the panel strength is influenced by wrinkling behavior and the procedures of case III are applied for correlating crippling strengths in the other materials. If the lower of the two predicted failing strengths for each panel is compared with the test value, satisfactory agreement is obtained in most cases.

The comparisons in table IV are for the panel of reference 15 having the smallest width-thickness ratios of its plate elements. The panel proportions and the R-value of 0.85 obtained in 7075-T6 aluminum alloy identify this panel as one in which both buckling and failure occur in the wrinkling mode. When the correlation procedure of case III is applied, the predicted strengths based on the material correlation parameter for wrinkling failures are seen to be in close agreement with the test data.

Because the test results of table IV all fall in the inelastic stress range for the materials where little or no margin is expected between buckling and maximum load, a valid objection is that the data should correlate with a buckling modulus irrespective of the mode of failure. A panel cross section was therefore designed which would undergo a wrinkling failure at a stress of about 30 ksi in a material having an elastic modulus of 10,500 ksi. Four panels were fabricated and duplicate tests were run in 2024-T3 and 7075-T6 aluminum alloy. The panel cross section and the test results are shown in figure 10. The predicted behavior of the panel for failure in the local buckling mode as well as for failure in the wrinkling mode are shown for comparison with the test data. This comparison clearly shows that a large change in yield stress in a panel material has little effect on panel crippling strength when the mode of failure is wrinkling.

The final comparison illustrates an approximation that simplifies the strength correlation for thick plates as found in multiweb-wing construction where a relatively small percentage of the total bending moment is carried by the supporting webs. The stress obtained by dividing the failure bending moment by the section modulus approximates the skin stress in construction of this type and tends to bear a constant ratio to it in beams of the same geometry but different material. Use of the more readily calculated M/S stress in place of the maximum average stress in the skin in a strength correlation is shown in table V. The M/S stresses at failure for the two beam cross sections illustrated were obtained in 7075-T6 aluminum alloy in tests at room temperature and after $\frac{1}{2}$-hour exposure to 250° F and 350° F. The M/S stresses for the beams in the room-temperature tests are somewhat larger than the maximum average stress for the compressive cover skins as read from figure 4; this condition indicates that an elevated-temperature strength prediction on the basis of the material correlation parameter for failure in the local buckling mode is appropriate. The elevated-temperature strength predictions were therefore performed in the manner illustrated in figure 5 by using the $\frac{1}{2}$-hour exposure, compressive stress-strain curves for the beam-cover skin material to construct the curves for the variation of $\sigma/(E_s\sigma_{cy})^{1/2}$ with σ. The predicted results at the elevated temperatures were read

from these curves at the values of $\sigma/(E_s\sigma_{cy})^{1/2}$ determined by the room-temperature test values of M/S for the two beam proportions. The results in table V, as well as those in figure 8, indicate that a high degree of accuracy is attainable in correlating the room- and elevated-temperature crippling strength of plate structures.

CONCLUDING REMARKS

A correlation approach to the crippling-strength analysis of multiplate-element structures in new materials and at elevated temperatures has been presented. The aim has been to lend confidence to the idea that, with suitable crippling-strength moduli and correlation procedures, established crippling-strength data in one material can be used as a basis for an accurate prediction of the behavior of geometrically similar structures having different material properties. The approach is particularly attractive for stiffened plate components where the effect of all the geometrical variables on crippling strength may not be as readily determined as the effect of a material property change. Even in the case of simpler structures, such as stiffener sections, the correlation approach may offer an advantage in speed as well as in accuracy. The strength analysis of structures in a new material may also be expedited by knowledge of the predicted behavior of structures of slightly different proportions the strengths of which have been definitely established by tests in another material.

A limitation of the present procedure is the possibility of a reduction in accuracy due to an unforeseen failure-mode change when the effect of a substantial increase in material yield strength to Young's modulus ratio is to be predicted. This limitation presents no handicap when the reference material for test data is 7075-T6 aluminum alloy but it may lead to surprises when dealing with test data accumulated in some of the lower strength materials. Fortunately, elevated-temperature strength predictions usually involve decreasing values of this ratio in which case the inherent accuracy of the correlation procedures is good.

The material correlation parameters discussed are all readily calculated from the effective compressive stress-strain curve for the material in the structure. Comparisons with available data indicate that a set of material parameters defined in this paper more accurately reflect the effect on structural strength of changes in the shape of stress-strain curves than parameters determined by the slope and 0.2 percent offset yield stress. In many practical situations, however, this improvement tends to be overshadowed by limitations on the accuracy with which the material properties in fabricated structures are known. When detailed data on material properties are available, utilization of this information

in the construction of effective material stress-strain curves for the structure leads to improved correlation accuracy.

Langley Aeronautical Laboratory,
National Advisory Committee for Aeronautics,
Langley Field, Va., October 4, 1955.

APPENDIX A

PLATE TESTS IN V-GROOVE EDGE FIXTURES

For the purpose of obtaining a direct comparison between plate compressive strength and the stress-strain curve for the plate material, tests were made on flat plates the side edges of which were supported in V-groove fixtures. Plates nominally 1/16 inch thick and having width-thickness ratios b/t ranging from 15 to 60 were tested. The plate length was such that five or more local buckles could form. The compressive stress-strain curves for the materials in the plates tested are shown in figure 2.

A schematic drawing of the V-groove fixtures is shown in figure 11. The grooves which support the side edges of the plate specimen are 1/4 inch deep and have a 60° included angle. A clamping force of about 100 pounds in each of the four clamping bolts was used to keep the plate side edges alined in the V-grooves. Preliminary tests showed that the maximum strength of the plates varied with clamping pressure but that a leveling off in strength occurred with a force of about 100 pounds in each bolt. Graphite lubrication of the grooves kept the sliding friction to a negligible quantity in the tests.

The behavior of plates in these fixtures may be described as follows: Buckling loads are obtained which are in agreement with those calculated for long plates with simply supported side edges. This load could be determined as the point at which the stress unit-shortening curve measured in a test deviated from the material stress-strain curve. In some tests, the top of the knee of the measured load—lateral-deflection curves was taken as the buckling load. Beyond buckling, lateral forces are exerted on the V-grooves by the plate edges which tend to separate the grooved support plates. The resulting misalinement of the plate edges in the grooves with increasing load leads to a maximum load which may be taken as characteristic of the plate b/t and the supporting fixture. Although the aim in the tests was to obtain comparable results among materials, the maximum stresses obtained were later determined to be in agreement with tests on square tubes and with the apparent maximum stresses of plates supported by longitudinal stiffeners, as in a crippling test on a short stiffened panel. This coincidence suggests that the support characteristics of this type of fixture are fairly representative of the support provided plates by the attachment flanges of riveted-on longitudinal stringers.

The test results obtained are given in table VI. They include the buckling and maximum stresses and the unit shortening (when measured) at the maximum of the load-shortening curve. Calculated values of σ_{cr},

obtained by assuming simply supported edges and $\eta = \sqrt{\frac{E_t}{E}}$, are given for comparison with the test values. In the case of the 18-8-$\frac{3}{4}$H stainless steel, the values of η were computed from the effective stress-strain curves of figure 2(f). The unit shortenings at failure show that, regardless of the stress for buckling, the maximum load for each plate was not reached until the longitudinal edges of the plate had been strained well into the inelastic stress range for the material.

The starred results shown in table VI are those chosen for presentation in figures 3 to 5. These results were considered to be representative of the strength of the plates in a given material as determined by the type of plot shown in figure 12 for all the test results in 7075-T6 aluminum alloy. The starred results in table VI for this material are indicated by flags in figure 12. The scatter in the results is believed to be characteristic of the test technique rather than caused by variations in material properties.

APPENDIX B

EFFECTIVE STRESS-STRAIN CURVES

In the manufacture of sheet metal parts, significant changes in material properties often occur. The increase in yield stress in the formed corners of stiffener sections, for example, is known to have a greater effect on the section's crippling stress than can be accounted for by the usually small increase in the area weighted average of the material properties over the section. An investigation of this problem in reference 5 showed that the changes in strength of formed sections were more nearly proportional to changes in material-strength moduli computed from stress-strain curves obtained by an equal weighting of the formed-corner stress-strain properties with those representative of the flat sheet. Such curves are called effective stress-strain curves in this paper.

The fact that strength moduli computed from effective, rather than average, stress-strain curves correlate with crippling-test data may be explained by the importance of material properties near the plate edges where the buckling distortions are least and the highest compressive stresses are reached. The effective stress-strain curve eliminates the need for assigning a crippling stress to small-radius corner elements as is done in most crippling-stress-analysis methods. The effective stress-strain curve is also adequate for computing both the elastic and inelastic buckling stresses inasmuch as it has the same initial slope as the average curve and has nearly the same shape as the average curve for sections which buckle in the inelastic range.

In order to correlate the strength of plates made of highly anisotropic materials, such as the 18-8-$\frac{3}{4}$H stainless steel plates tested in this investigation, the concept of an effective stress-strain curve can also be used to advantage. It was found that plates with the same width-thickness ratio cut from the with-grain and cross-grain directions of the rolled sheet failed at the same value of $\frac{\sigma}{(E_s\sigma_{cy})^{1/2}}$ when $(E_s\sigma_{cy})^{1/2}$ was computed from a weighted average of the material stress-strain curves for the loading direction and transverse direction. The stress-strain curve in the loading direction was weighted twice as heavily as the curve in the transverse direction. With an effective stress-strain curve defined in this manner, the data for 18-8-$\frac{3}{4}$H stainless steel correlate with the data for more nearly isotropic materials, as shown in figure 4.

For structural sections formed of an anisotropic material, the effective stress-strain curve for the flat material is averaged with a stress-strain curve for the formed-corner material (loading direction) to obtain an effective stress-strain curve for the section.

APPENDIX C

MATERIAL STRENGTH MODULI

The influence of material on the crippling strength of plate structures has been represented by material parameters which are a function of material stress-strain curve slope and height. The relative weight given to each of these material characteristics ought to be related to the stress—unit-shortening diagram for the structure in question. An approximate relationship can be obtained from a consideration of figure 13 where stress—unit-shortening diagrams are drawn for three different structures which have the same elastic buckling stress. These diagrams are shown superposed on the material stress-strain curve.

Each of the stress—unit-shortening curves in figure 13 can be approximated by an equation of the form

$$\frac{\bar{\sigma}}{\sigma_e} = \left(\frac{\epsilon_{cr}}{\epsilon_e}\right)^{1-m} \tag{C1}$$

where m is the ratio of the initial slope of the stress—unit-shortening curve after buckling to the initial slope of the stress-strain curve and ϵ_{cr} is the buckling strain. Equation (C1) can be solved for the maximum average stress $\bar{\sigma}_f$ as follows:

$$\bar{\sigma}_f = \left(\frac{\sigma_e'}{\epsilon_e^{1-m}}\right)_{max} \epsilon_{cr}^{1-m} = \left(E_s^{1-m}\sigma_e^{m}\right)_{max} \epsilon_{cr}^{1-m} \tag{C2}$$

which is associated with the maximum value of $\left(E_s^{1-m}\sigma_e^{m}\right)$. For a value of m, a maximum value of $\left(E_s^{1-m}\sigma_e^{m}\right)$ can be determined from the material stress-strain curve by satisfying the relationship

$$\left.\begin{aligned} \frac{d\sigma}{d\epsilon} &= (1-m)\frac{\sigma}{\epsilon} \\ \text{or} \qquad E_t &= (1-m)E_s \end{aligned}\right\} \tag{C3}$$

Equations (C2) and (C3) show that as m changes from 0 to 1 the maximum stress depends less upon stress-strain curve slope and more upon the magnitude of the stresses attainable in the material. This result is in qualitative agreement with the observed behavior of actual structures; that is, the maximum strength of a Euler column, for which m is zero, depends on the stress-strain curve slope whereas the maximum strength of plate structures, which have m values between 0 and 1, depend also upon the height of the material stress-strain curve beyond the stress at which buckling initiates in the structure. The trend of equation (C2), rather than the precise weighting of material stress-strain curve characteristics for any m value, is considered of significance in establishing material strength moduli for various structures and their modes of failure.

The strength moduli employed in this paper are associated with values of m equal to 1/2 and 2/3. When m is equal to 1/2, the strength modulus $(E_s'\sigma_2)^{1/2}$ is obtained, where σ_2 is the stress at which the tangent is one-half the secant modulus and E_s' is the secant modulus at σ_2. The strength modulus $(E_s'\sigma_3^2)^{1/3}$ is associated with $m = 2/3$; σ_3 is the stress at which the tangent is one-third the secant modulus and E_s' is the secant modulus at σ_3. Parameters could be defined in a similar manner for other values of m.

The parameters $(E_s\sigma_{cy})^{1/2}$ and $(E_s\sigma_{cy}^2)^{1/3}$ may be considered as versions of the preceding parameters employing more commonly known material characteristics. With most materials the latter parameters are approximately proportional to the preceding ones.

REFERENCES

1. Von Kármán, Theodor, Sechler, Ernest E., and Donnell, L. H.: The Strength of Thin Plates in Compression. A.S.M.E. Trans., APM-54-5, vol. 54, no. 2, Jan. 30, 1932, pp. 53-57.

2. Heimerl, George J.: Determination of Plate Compressive Strengths. NACA TN 1480, 1947.

3. Schuette, E. H.: Observations on the Maximum Average Stress of Flat Plates Buckled in Edge Compression. NACA TN 1625, 1949.

4. Needham, Robert A.: The Ultimate Strength of Aluminum-Alloy Formed Structural Shapes in Compression. Jour. Aero. Sci., vol. 21, no. 4, Apr. 1954, pp. 217-229.

5. Anderson, Melvin S.: Compressive Crippling of Structural Sections. NACA TN 3553, 1955.

6. Semonian, Joseph W., and Anderson, Roger A.: An Analysis of the Stability and Ultimate Bending Strength of Multiweb Beams With Formed-Channel Webs. NACA TN 3232, 1954.

7. Conway, William J.: Factors Affecting the Design of Thin Wings. Preprint No. 357, SAE Los Angeles Aero. Meeting; Oct. 5-9, 1954.

8. Semonian, Joseph W., and Peterson, James P.: An Analysis of the Stability and Ultimate Compressive Strength of Short Sheet-Stringer Panels With Special Reference to the Influence of Riveted Connection Between Sheet and Stringer. NACA TN 3431, 1955.

9. Gallaher, George L.: Plate Compressive Strength of FS-1h Magnesium-Alloy Sheet and a Maximum-Strength Formula for Magnesium-Alloy and Aluminum-Alloy Formed Sections. NACA TN 1714, 1948.

10. Pride, Richard A., and Heimerl, George J.: Plastic Buckling of Simply Supported Compressed Plates. NACA TN 1817, 1949.

11. Crockett, Harold B.: Predicting Stiffener and Stiffened Panel Crippling Stresses. Jour. Aero. Sci., vol. 9, no. 13, Nov. 1942, pp. 501-509.

12. Heimerl, George J., and Roberts, William M.: Determination of Plate Compressive Strengths at Elevated Temperatures. NACA Rep. 960, 1950. (Supersedes NACA TN 1806.)

13. Bijlaard, P. P., and Johnston, G. S.: Compressive Buckling of Plates Due to Forced Crippling of Stiffeners. Parts I and II. S.M.F. Fund Paper No. FF-8, Inst. Aero. Sci., Jan. 1953.

14. Argyris, J. H., and Dunne, P. C.: Part 2. Structural Analysis. Structural Principles and Data, Handbook of Aeronautics, No. 1, Pitman Pub. Corp. (New York), 1952, pp. 77-317.

15. Dow, Norris F., Hickman, William A., and Rosen, B. Walter: Data on the Compressive Strength of Skin-Stringer Panels of Various Materials. NACA TN 3064, 1954.

16. Schuette, Evan H.: Charts for the Minimum-Weight Design of 24S-T Aluminum-Alloy Flat Compression Panels With Longitudinal Z-Section Stiffeners. NACA Rep. 827, 1945. (Supersedes NACA WR L-197.)

17. Hickman, William A., and Dow, Norris F.: Compressive Strength of 24S-T Aluminum-Alloy Flat Panels With Longitudinal Formed Hat-Section Stiffeners Having Four Ratios of Stiffener Thickness to Skin Thickness. NACA TN 1553, 1948.

18. Hickman, William A., and Dow, Norris F.: Data on the Compressive Strength of 75S-T6 Aluminum-Alloy Flat Panels Having Small, Thin, Widely Spaced, Longitudinal Extruded Z-Section Stiffeners. NACA TN 1978, 1949.

19. Hickman, William A., and Dow, Norris F.: Data on the Compressive Strength of 75S-T6 Aluminum-Alloy Flat Panels With Longitudinal Extruded Z-Section Stiffeners. NACA TN 1829, 1949.

TABLE I

PROPERTIES OF PLATE MATERIALS

Material	$(E\sigma_{cy})^{1/2}$ ksi	$(E_s\sigma)^{1/2}_{max}$, ksi	$\frac{(E_s\sigma)^{1/2}_{max}}{(E\sigma_{cy})^{1/2}}$
FS-1h magnesium alloy	416	367	0.88
2024-T3 aluminum alloy . . .	681	592	.87
2014-T6 aluminum alloy . . .	810	744	.92
7075-T6 aluminum alloy . . .	873	803	.92
Stainless W steel	2,420	2,200	.92
18-8-$\frac{3}{4}$H stainless steel			
Effective with grain . . .	1,880	1,560	.83
Effective cross grain . . .	2,020	1,710	.85

TABLE II

COMPARISON OF PREDICTIONS WITH TEST RESULTS FOR

Z-STIFFENED PANEL 37.5-75 OF REFERENCE 15

[7075-T6 reference panel; $R = \frac{29.8\ (1.58 + 1.43)}{(1.58)(22) + (1.43)(39)} = 0.99$ (eq. 6)]

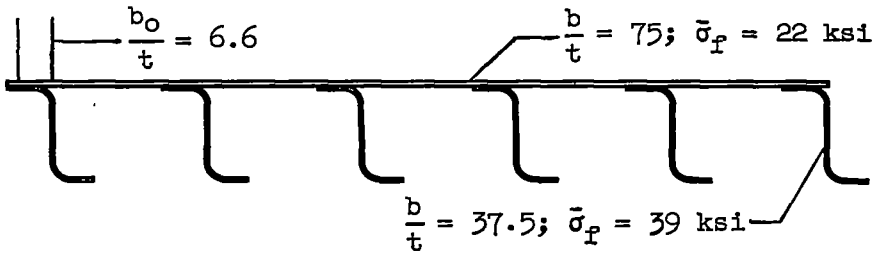

Material	$(\bar{\sigma}_f)_{test}$, ksi	$(\bar{\sigma}_f)_{predicted}$, ksi
6061-T6 aluminum alloy . . .	23.2	22.6
5052-$\frac{1}{4}$H aluminum alloy . . .	16.5	16.4
7075-0 aluminum alloy . . .	11.6	13.3
SAE 1010 steel	24.0	25.1
Copper	19.2	21.1
FS-1h magnesium alloy . . .	14.0	13.4
18-8-$\frac{3}{4}$H steel*	58.2	66.4
Ti-$\frac{1}{4}$H steel	37.5	35.7

*This panel has a value of b_o/t 10 percent larger than the reference panel.

TABLE III

COMPARISON OF PREDICTIONS WITH TEST RESULTS FOR

Z-STIFFENED PANEL 18.75-37.5 OF REFERENCE 15

[7075-T6 reference panel; $R = \dfrac{50.8\,(0.81 + 0.78)}{(0.81)(37) + (0.78)(76)} = 0.91$ (eq. 6)]

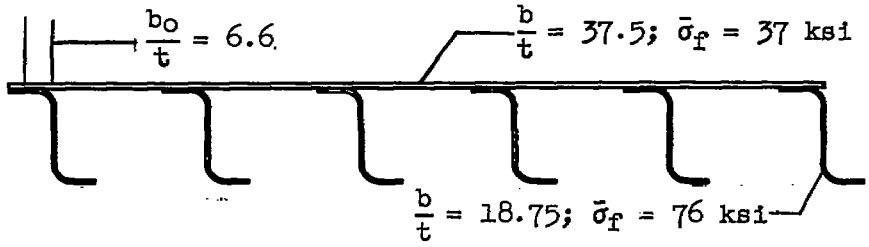

Material	$(\bar{\sigma}_f)_{test}$, ksi	$(\bar{\sigma}_f)_{predicted}$, ksi	
		Failure in local buckling mode	Failure in wrinkling mode
6061-T6 aluminum alloy . . .	34.2	37.5	37.6
5052-$\frac{1}{4}$H aluminum alloy . . .	22.5	24.7	23.6
7075-0 aluminum alloy . . .	17.0	18.7	17.7
SAE 1010 steel	32.6	31.8	30.5
Copper	27.4	29.1	27.6
FS-1h magnesium alloy . . .	20.1	22.3	22.0
18-8-$\frac{3}{4}$H steel*	93.1	116.7	107
Ti-$\frac{1}{4}$H steel	64.5	62.4	57.5

*This panel has a value of b_o/t 10 percent larger than the reference panel.

TABLE IV

COMPARISON OF PREDICTIONS WITH TEST RESULTS FOR

Z-STIFFENED PANEL 12.5-25 OF REFERENCE 15

[7075-T6 reference panel; $R = \frac{60.4\ (0.55 + 0.57)}{(0.55)(0.59) + (0.57)(82)} = 0.85$ (eq. 6)]

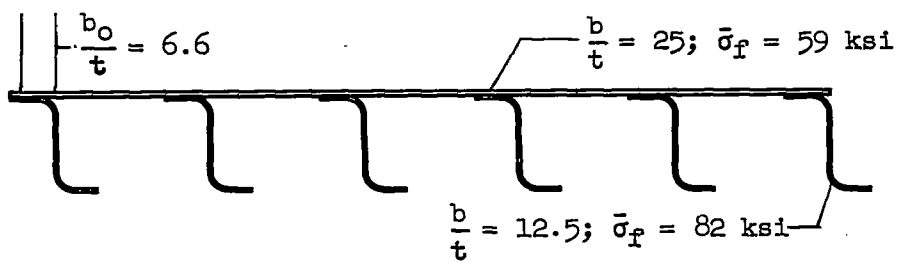

Material	$(\bar{\sigma}_f)_{test}$, ksi	$(\bar{\sigma}_f)_{predicted}$, ksi
6061-T6 aluminum alloy . . .	40.1	40.1
5052-$\frac{1}{4}$H aluminum alloy . . .	25.8	25.4
7075-0 aluminum alloy . . .	20.9	19.9
SAE 1010 steel	35.9	32.7
Copper	30.1	29.1
FS-1h magnesium alloy . . .	23.4	24.1
18-8-$\frac{3}{4}$H steel*	116.2	126
Ti-$\frac{1}{4}$H steel	73.3	66.6

*This panel has a value of b_o/t 10 percent larger than the reference panel.

TABLE V

COMPARISON OF PREDICTION WITH TEST RESULTS FOR 7075-T6 ALUMINUM-ALLOY MULTIWEB BEAMS TESTED IN PURE BENDING AT ELEVATED TEMPERATURES

(a) Room-temperature reference beam; $\bar{\sigma}_f = \frac{M}{S} = 62.4$ ksi

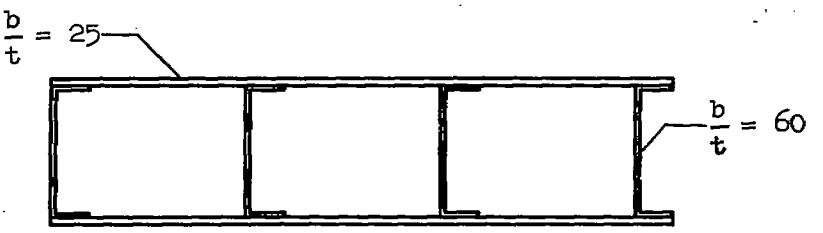

Temperature, °F	$(\bar{\sigma}_f)_{test}$, ksi	$(\bar{\sigma}_f)_{predicted}$, ksi
250	52.6	52.5
350	45.0	44.5

(b) Room-temperature reference beam; $\bar{\sigma}_f = \frac{M}{S} = 43.4$ ksi

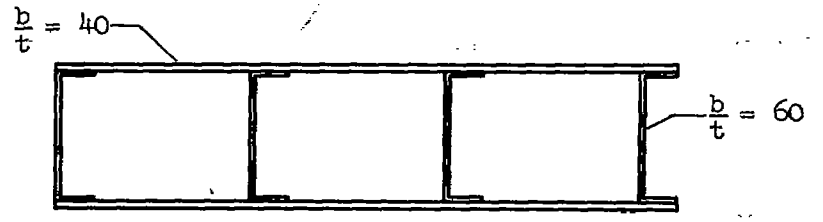

Temperature, °F	$(\bar{\sigma}_f)_{test}$, ksi	$(\bar{\sigma}_f)_{predicted}$, ksi
250	37.8	37.0
350	30.0	32.3

TABLE VI

PLATE TEST RESULTS

b/t	σ_{cr}, ksi	Calculated σ_{cr}, ksi	$\bar{\sigma}_f$, ksi	$\bar{\epsilon}_f$
FS-1h magnesium alloy				
20.0	25.1	26.3	25.1	0.00526
20.2*	25.9	26.3	25.9	.00568
20.1	25.7	26.3	25.7	.00559
24.4	26.1	25.0	26.1	.00604
24.5	25.3	25.0	25.3	.00558
24.4*	24.9	25.0	24.9	.00532
33.0	18.1	19.2	19.2	.00328
32.8*	18.7	19.3	19.5	.00328
32.8	19.3	19.3	19.8	.00332
40.9*	13.6	14.1	15.4	.00302
41.0	14.1	14.0	15.7	.00307
41.4	13.2	13.7	15.6	.00313
2024-T3 aluminum alloy				
17.3	48.5	48.1	48.5	0.00920
17.4	44.5	47.8	44.5	.00675
17.4*	44.7	47.8	44.7	.00665
20.3	41.3	42.7	41.3	.00555
20.2	41.1	42.8	41.1	.00555
20.2*	43.6	42.8	43.6	.00658
25.2	36.2	38.0	36.8	.00445
25.0	38.6	38.2	38.6	.00485
25.2*	38.4	38.0	38.9	.00530
30.6	33.5	33.3	34.4	.00355
30.6	33.2	33.3	34.1	.00355
30.9*	32.6	33.1	33.2	.00345
40.8	23.3	23.4	25.9	.00390
40.6	23.1	23.5	25.5	.00380
40.6*	23.6	23.5	25.8	.00390
50.6	15.3	15.1	22.2	.00490
50.4*	15.4	15.3	22.1	.00455
50.7	15.8	15.1	22.3	.00500
2014-T6 aluminum alloy				
20.8*	60.8	57.0	61.0	-------
22.5*	57.8	54.8	57.9	-------
25.6*	53.3	52.3	53.9	-------
30.1*	42.9	42.8	43.5	-------
42.5*	22.0	21.5	31.5	-------

*Points that are plotted in figures 4, 5, and 6.

4, 6, & 7 ?

TABLE VI.- Continued

PLATE TEST RESULTS

b/t	σ_{cr}, ksi	Calculated σ_{cr}, ksi	$\bar{\sigma}_f$, ksi	$\bar{\epsilon}_f$
7075-T6 aluminum alloy				
14.7	70.5	76.0	71.0	0.00960
14.7*	77.6	76.0	77.6	.01075
14.6	73.4	76.1	75.4	.01100
16.4*	73.4	73.5	73.4	-------
16.4	72.2	73.5	72.2	-------
18.1	71.5	71.0	71.5	-------
18.1	71.6	71.0	71.6	-------
19.4	72.3	68.7	72.3	.00910
19.5	69.0	68.6	69.0	.00830
19.5*	70.1	68.6	70.1	.00888
20.6	66.5	66.6	66.5	-------
20.6	67.3	66.6	67.3	-------
24.5	59.6	59.7	59.6	.00690
24.3*	60.6	60.0	60.6	.00680
24.5	61.1	59.7	61.1	-------
25.7	52.9	57.6	52.9	-------
25.7	56.2	57.6	56.2	-------
29.0	41.6	45.2	48.1	.00510
28.8	42.6	45.8	46.5	.00485
29.2*	47.0	44.5	49.1	.00556
34.1	34.0	32.7	40.8	.00650
34.1*	34.7	32.7	40.5	.00692
34.0	35.2	32.9	40.5	.00675
36.7	28.9	28.2	37.4	-------
36.8	29.0	28.8	37.5	-------
38.8	26.1	25.2	37.0	.00685
39.0	26.5	25.0	37.1	.00720
38.4*	26.1	25.8	36.0	.00700
48.0*	15.0	16.5	30.3	.00790
48.5	15.7	16.2	30.6	.00730
48.2	15.2	16.3	31.1	.00785
51.5*	15.0	14.3	29.1	-------
58.0	12.3	11.3	26.9	.00690
58.2*	11.6	11.2	26.3	.00665
58.1	11.8	11.3	26.0	.00715

*Points that are plotted in figures 4, 5, and 6.

TABLE VI.- Concluded

PLATE TEST RESULTS

b/t	σ_{cr}, ksi	Calculated σ_{cr}, ksi	$\bar{\sigma}_f$, ksi	$\bar{\epsilon}_f$
Stainless W steel				
16.4*	201.0	193	202.0	0.00914
16.4	201.0	193	202.0	.00905
18.2*	199.5	187.2	201.0	.00913
18.4	187.3	186.6	187.3	.00811
21.2*	176.0	175.1	177.0	.00770
20.7	178.0	177.6	179.3	.00778
26.0	151.5	146.5	152.0	.00509
25.9*	148.0	147.4	148.3	.00521
36.5*	78.5	81.5	106.0	.00886
36.5	73.5	81.5	102.7	.00732
52.0*	36.3	40.2	78.6	.00739
18-8-$\frac{3}{4}$H stainless steel with grain				
19.2	146.8	142.0	146.8	-------
19.2*	140.5	142.0	140.5	-------
21.4	115.7	130.1	115.7	-------
21.5*	126.3	129.5	126.3	-------
24.7	107.7	112.9	107.7	-------
23.9*	111.8	116.7	111.8	-------
29.7	78.9	90.1	78.9	-------
29.6*	91.4	90.6	91.4	-------
42.7*	52.0	52.0	62.3	-------
42.5	49.8	52.2	61.0	-------
59.1*	26.4	28.0	49.6	-------
18-8-$\frac{3}{4}$H stainless steel cross grain				
19.1*	157.7	153.4	157.7	-------
19.1	153.0	153.4	153.0	-------
21.2	143.8	142.3	143.8	-------
21.2*	143.0	142.3	143.0	-------
24.0*	131.0	126.2	131.0	-------
24.3	138.2	124.5	138.2	-------
29.9	94.5	95.3	95.2	-------
29.9*	103.2	95.3	103.2	-------
42.2	52.5	54.2	69.3	-------
42.4*	55.4	53.5	71.6	-------
60.2*	27.9	29.0	55.3	-------

*Points that are plotted in figures 4, 5, and 6.

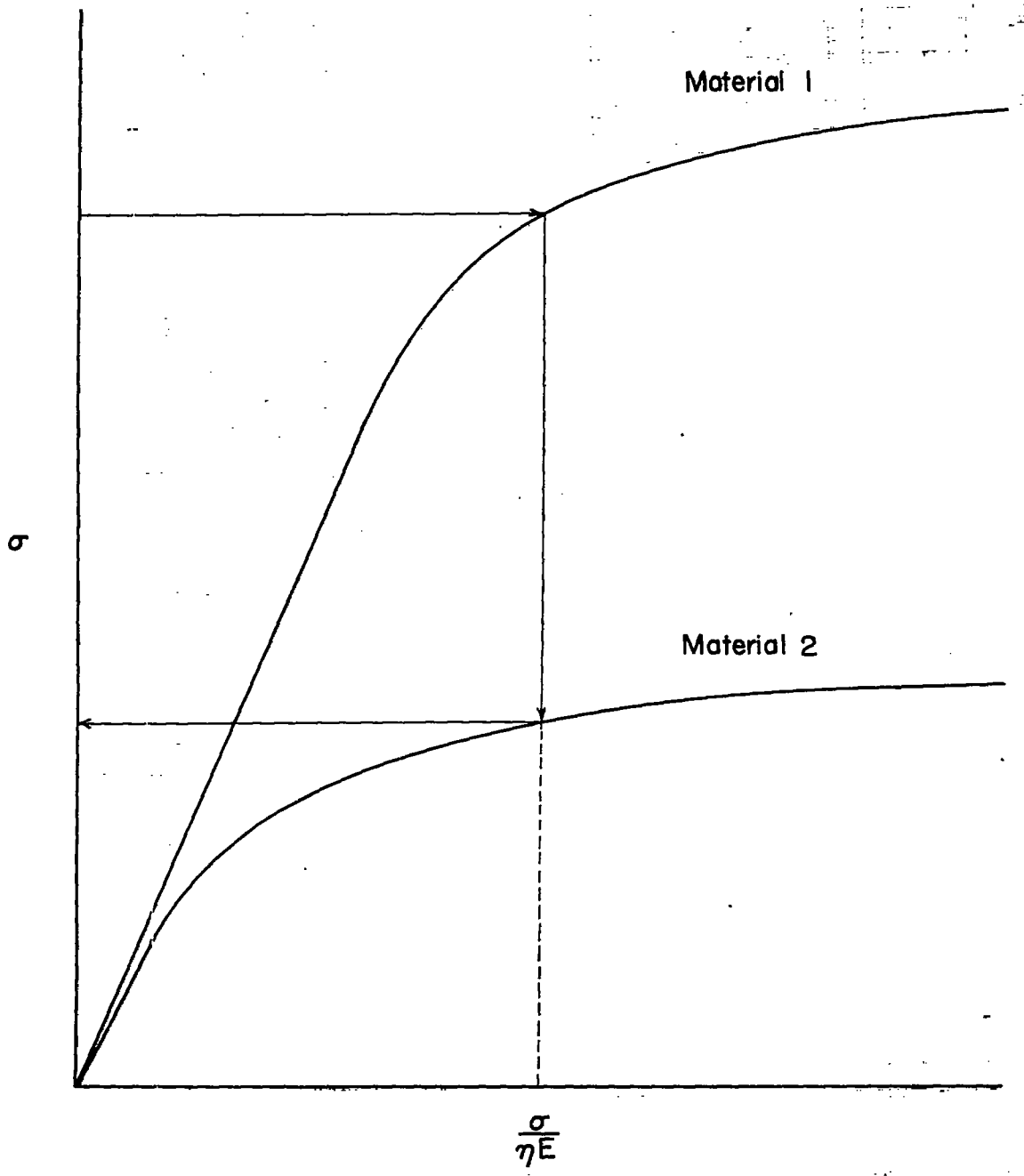

Figure 1.- Correlation procedure for plate buckling.

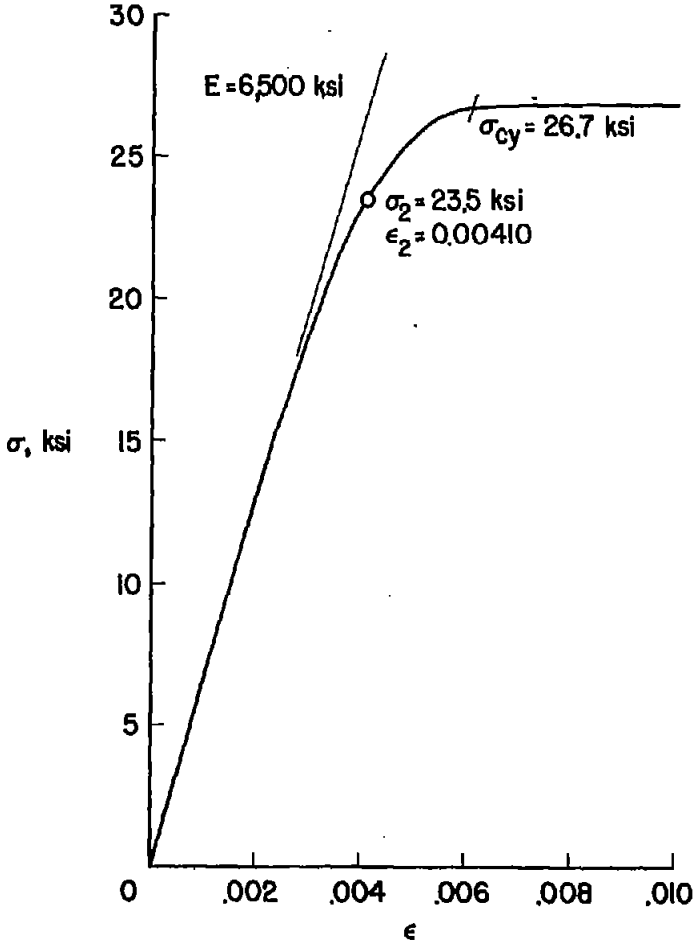

(a) FS-1H magnesium alloy.

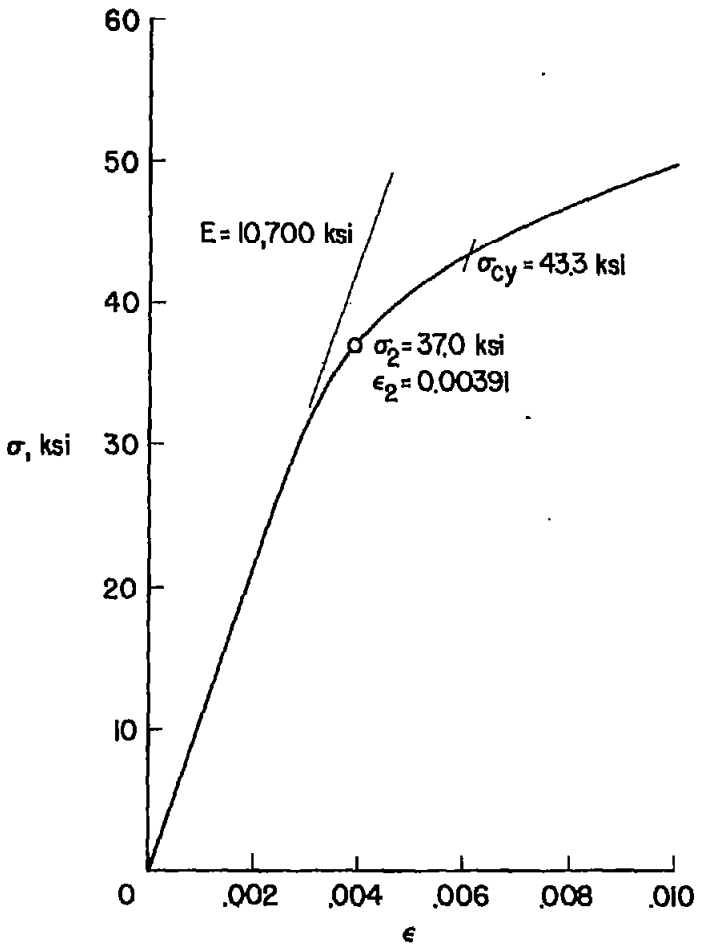

(b) 2024-T3 aluminum alloy.

Figure 2.- Compressive stress-strain curves for plates tested.

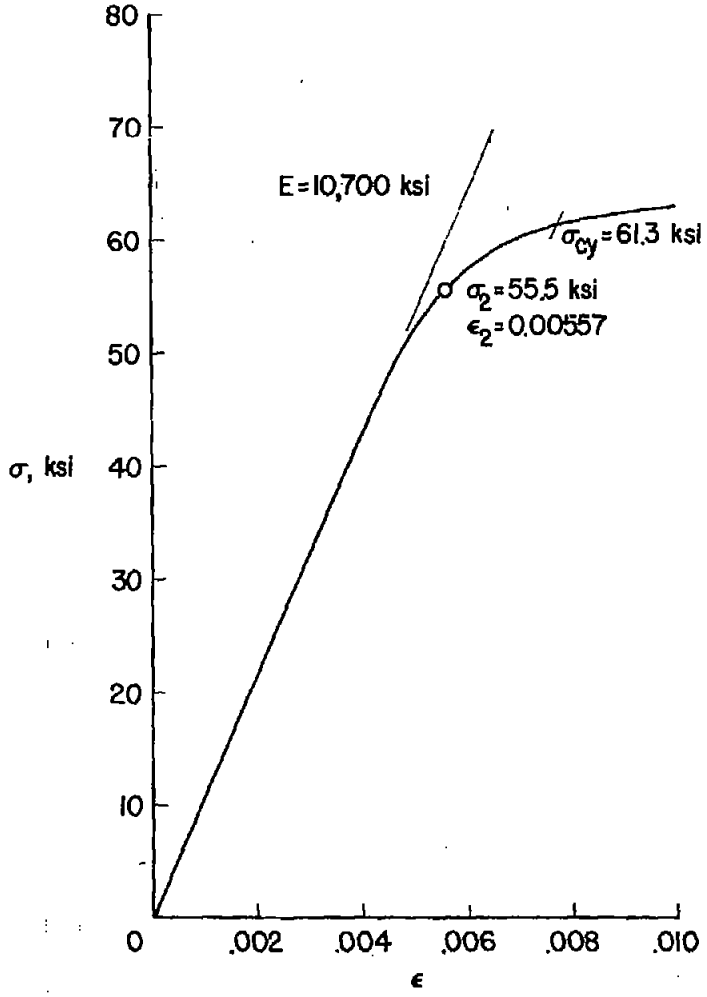

(c) 2014-T6 aluminum alloy.

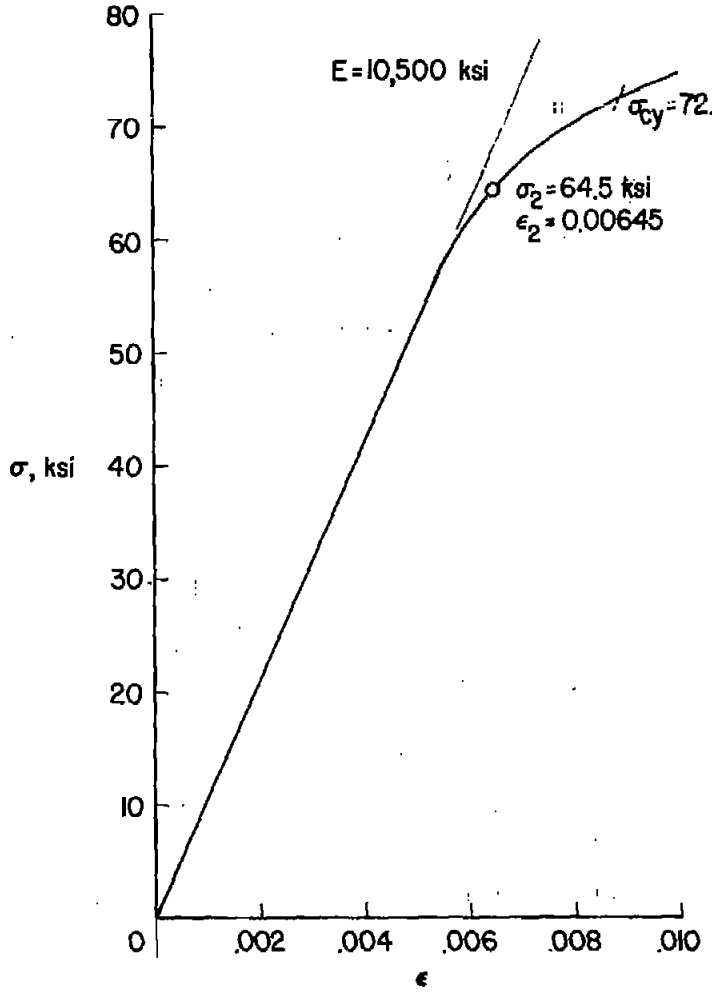

(d) 7075-T6 aluminum alloy.

Figure 2.- Continued.

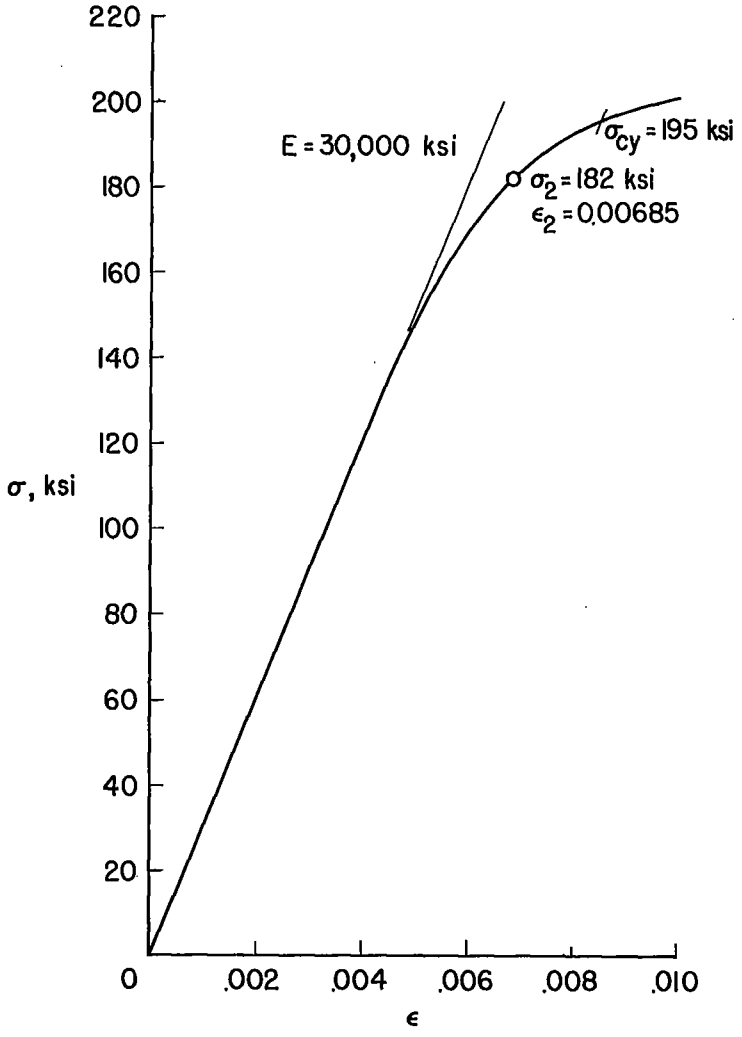

(e) Stainless W steel.

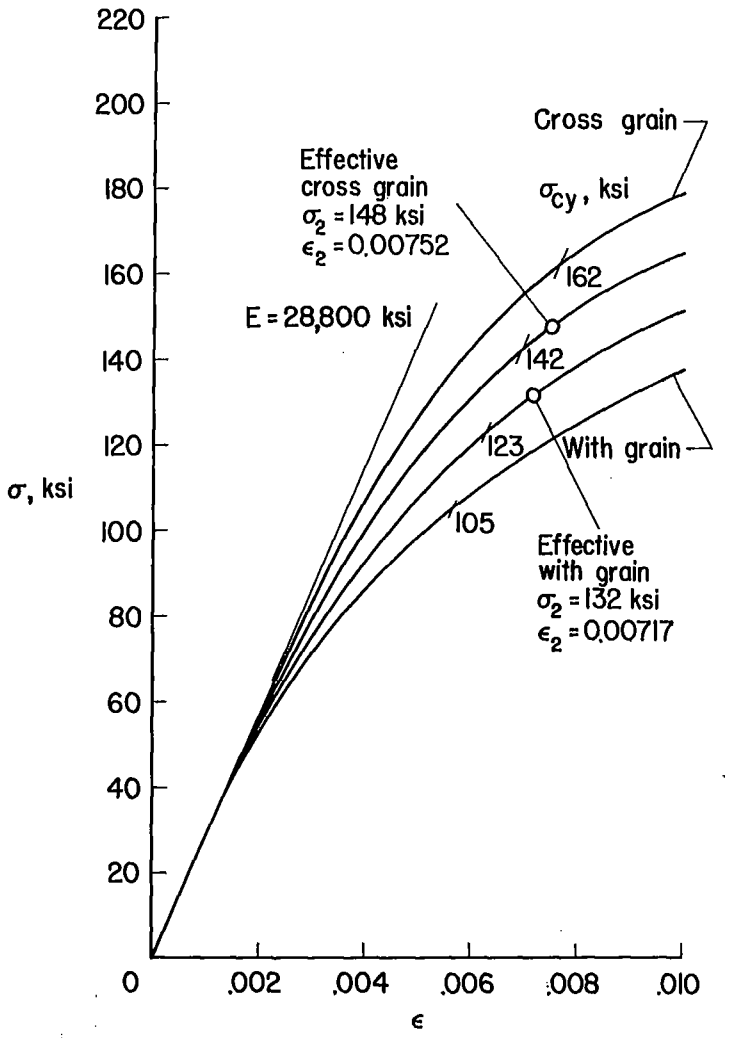

(f) 18-8-3/4H stainless steel.

Figure 2.- Concluded.

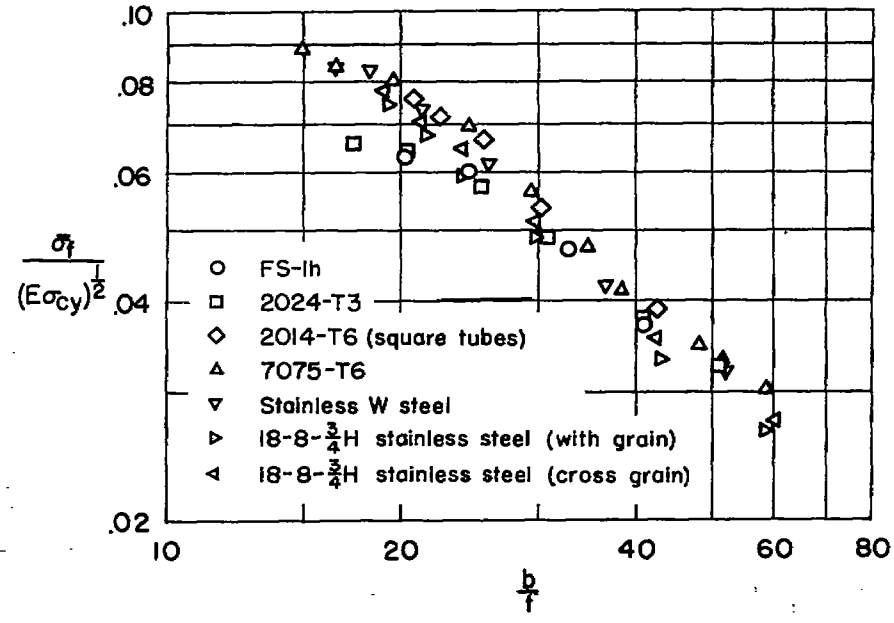

(a) $\left(E\sigma_{cy}\right)^{1/2}$.

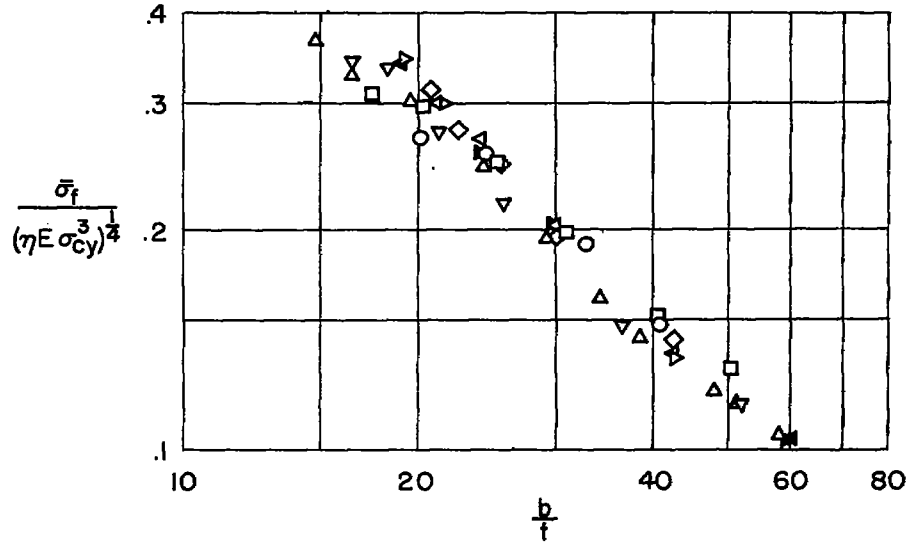

(b) $\left(\eta E\sigma_{cy}^{3}\right)^{1/4}$.

Figure 3.- Comparison of plate-strength data with previously proposed material parameters.

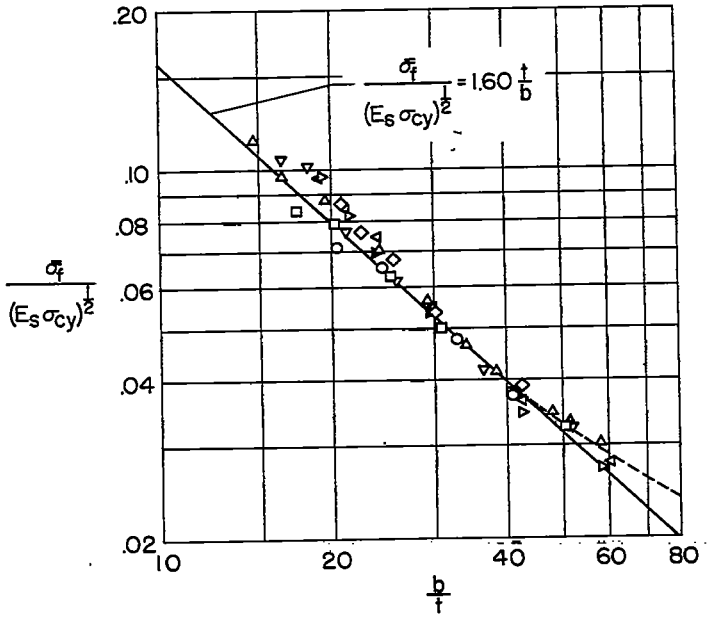

(a) $\left(E_s\sigma_{cy}\right)^{1/2}$.

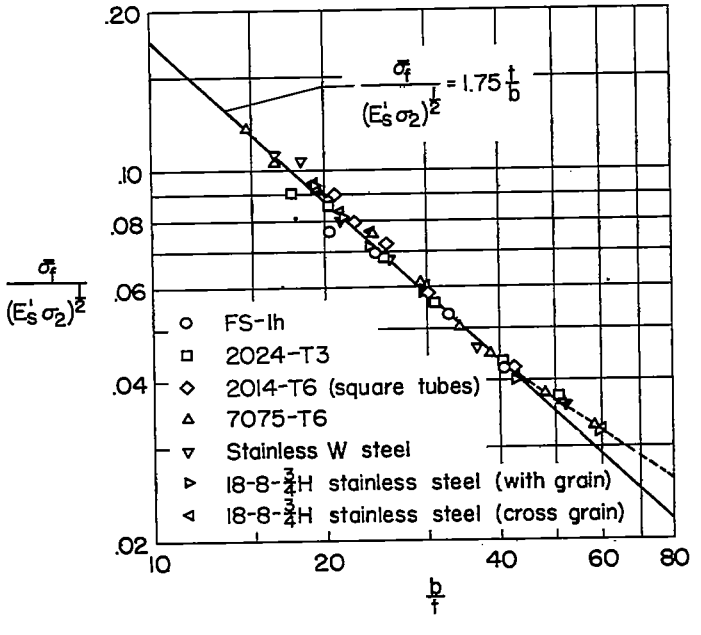

(b) $\left(E_s'\sigma_2\right)^{1/2}$.

Figure 4.- Comparison of plate-strength data with strength moduli.

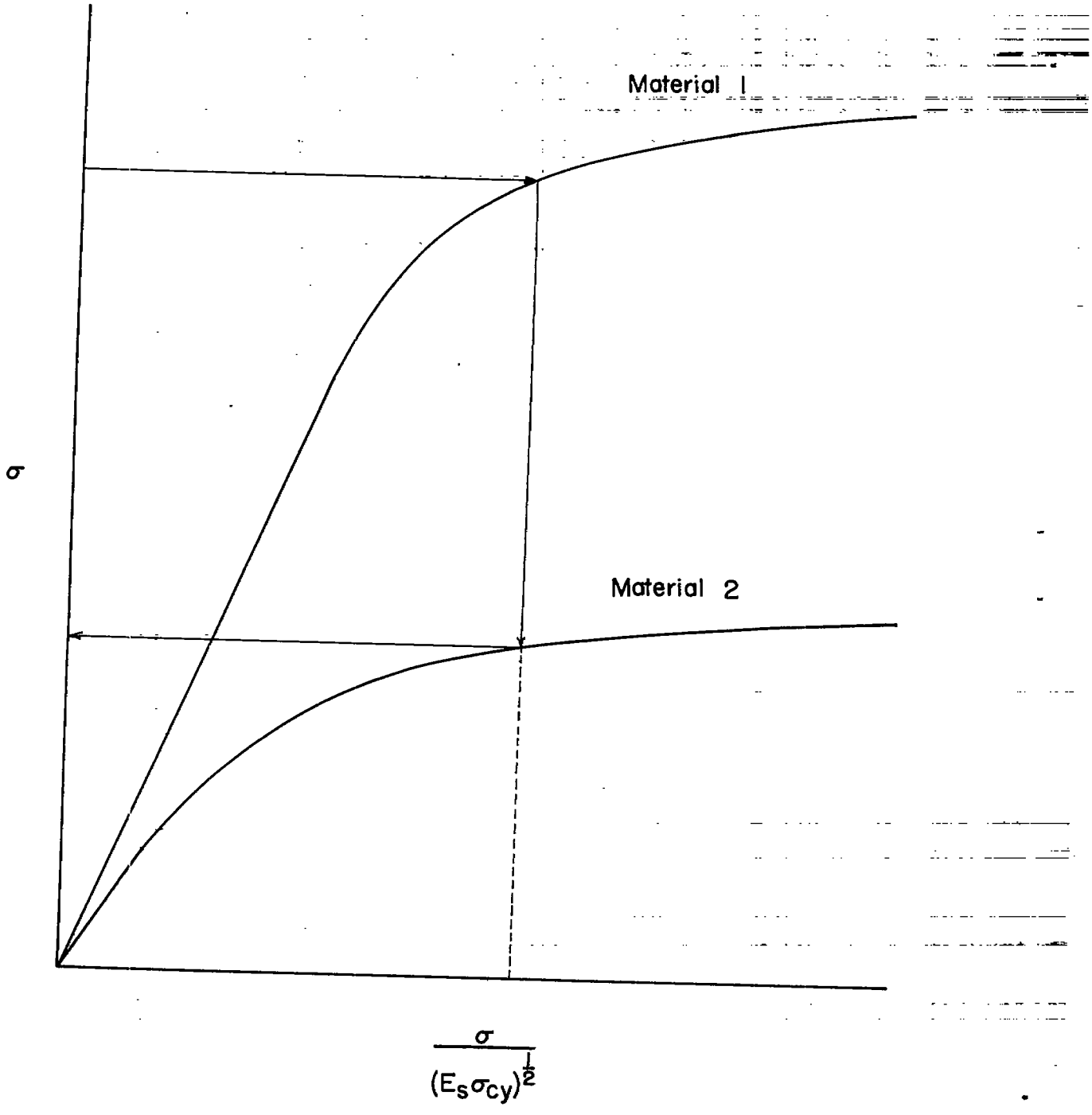

Figure 5.- Correlation procedure for failure in local buckling mode.

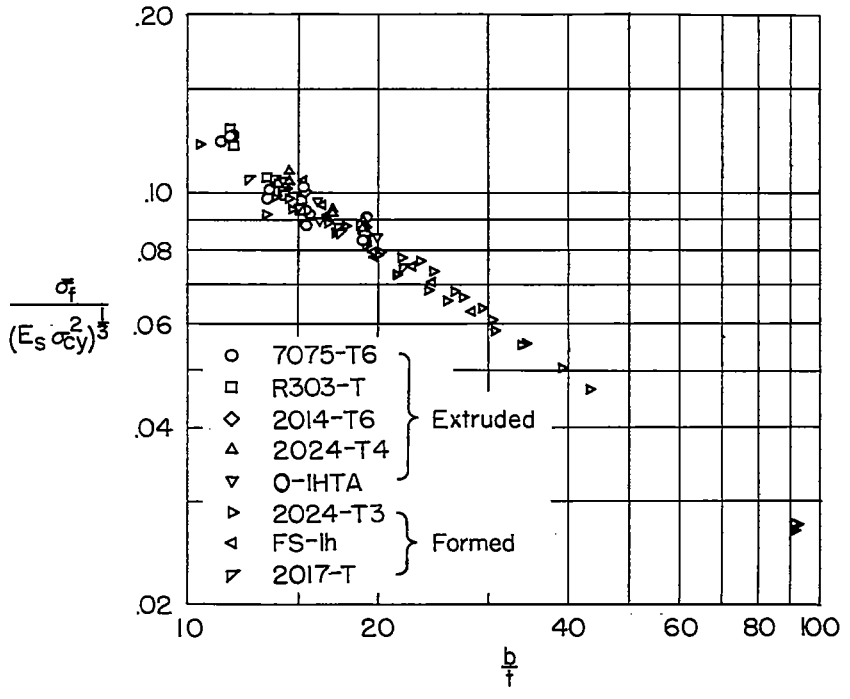

(a) $\left(E_s \sigma_{cy}^2\right)^{1/3}$.

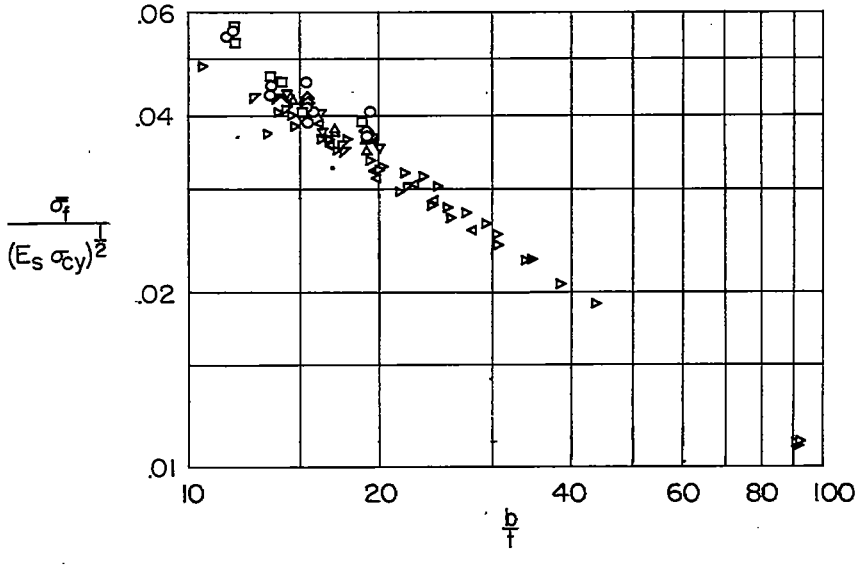

(b) $\left(E_s \sigma_{cy}\right)^{1/2}$.

Figure 6.- Comparison of flange crippling-strength data with strength moduli.

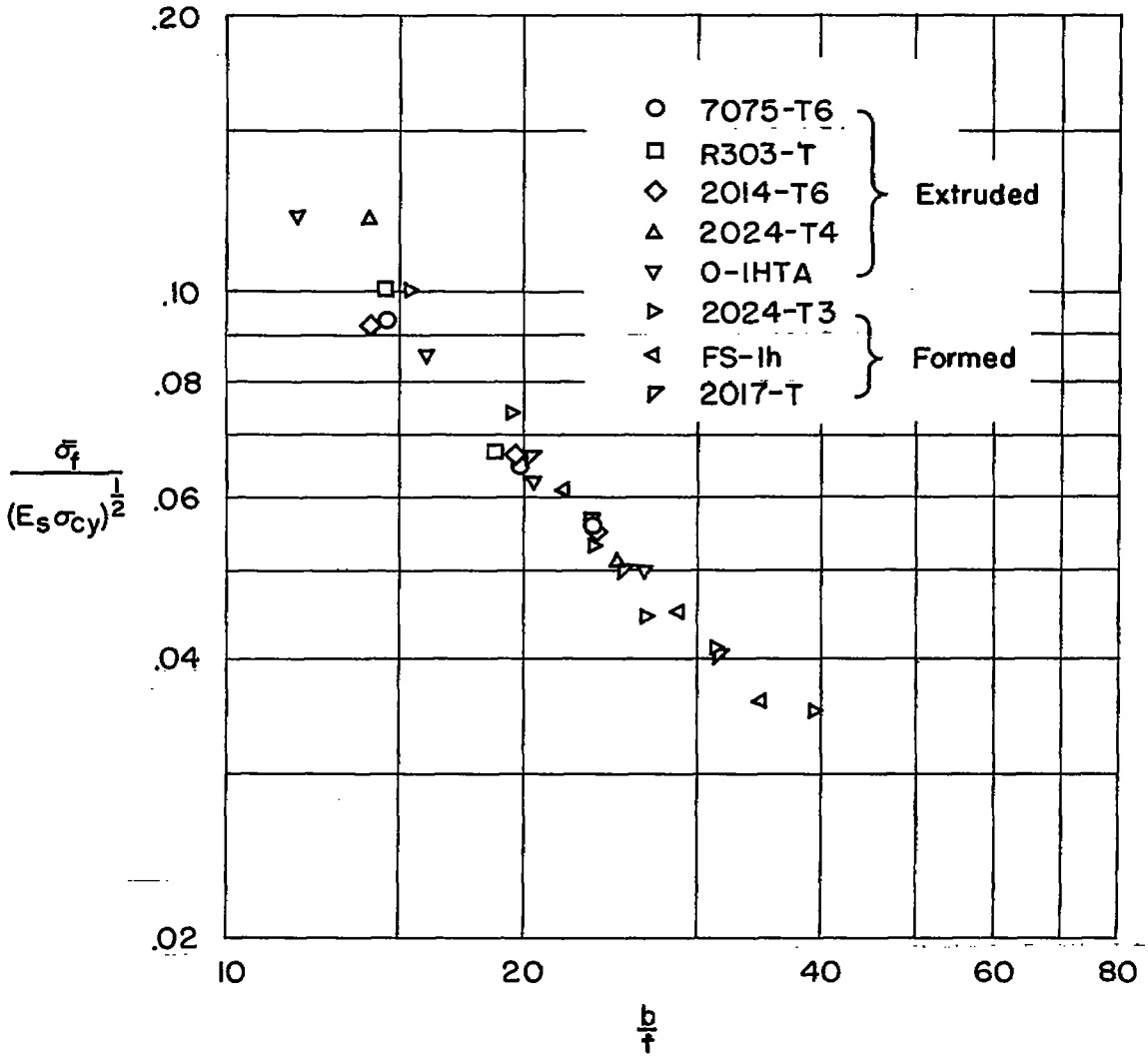

Figure 7.- Comparison of stiffener crippling-strength data with strength modulus. Z-section stiffeners have ratio of flange to web width of 0.6.

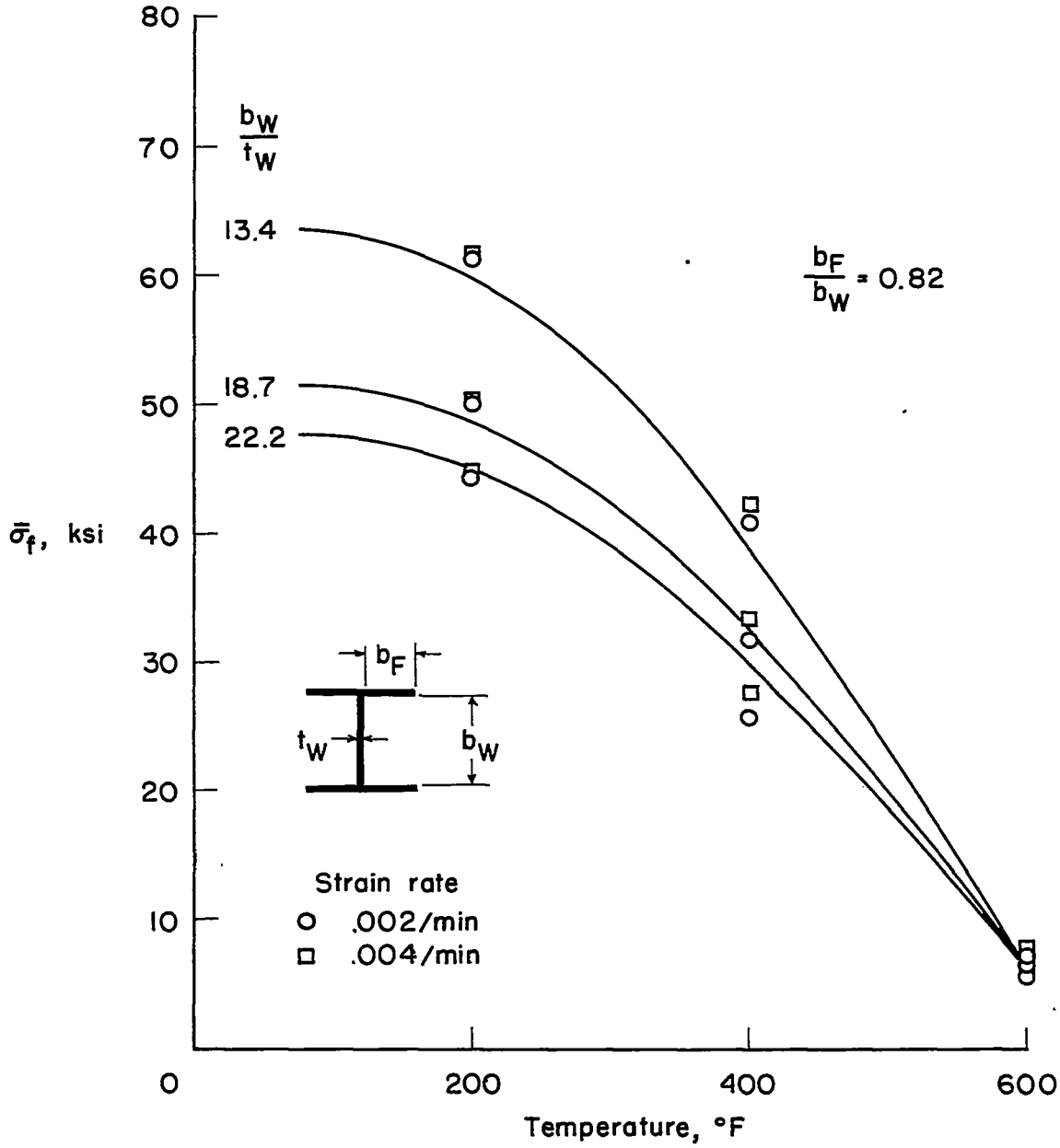

Figure 8.- Comparison of predicted elevated-temperature strength with test data for three H-sections. 7075-T6 aluminum alloy.

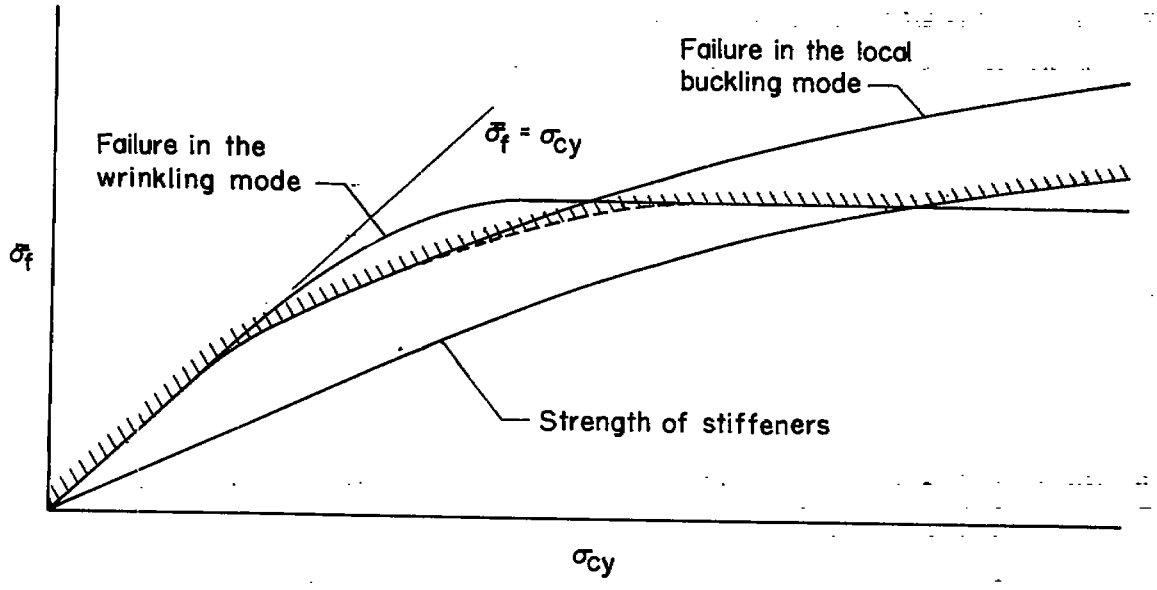

(a) E constant.

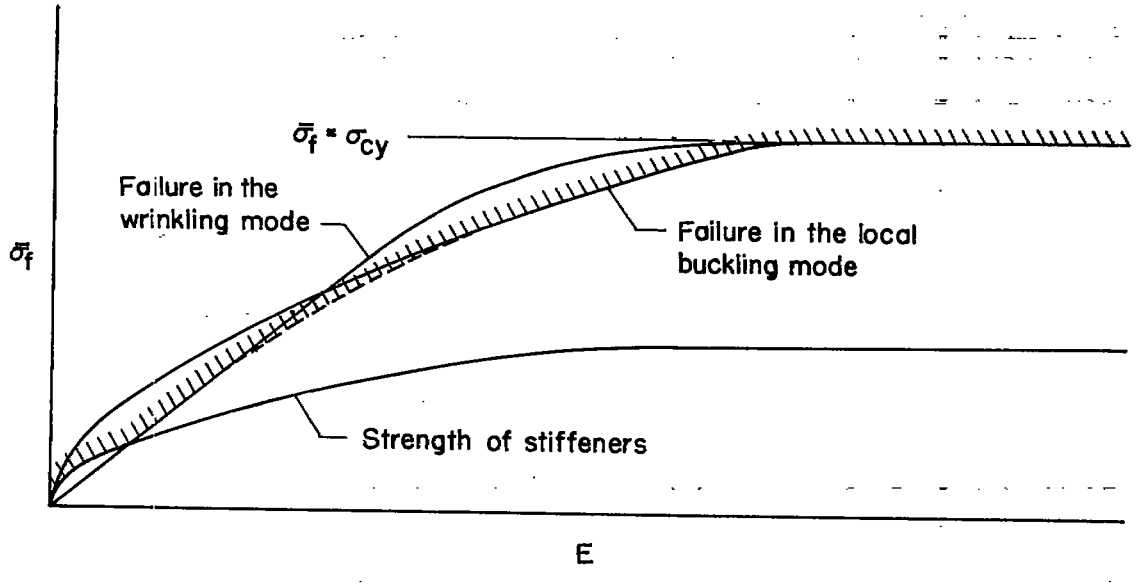

(b) σ_{cy} constant.

Figure 9.- Variation in crippling stress of a stiffened plate as material properties are changed.

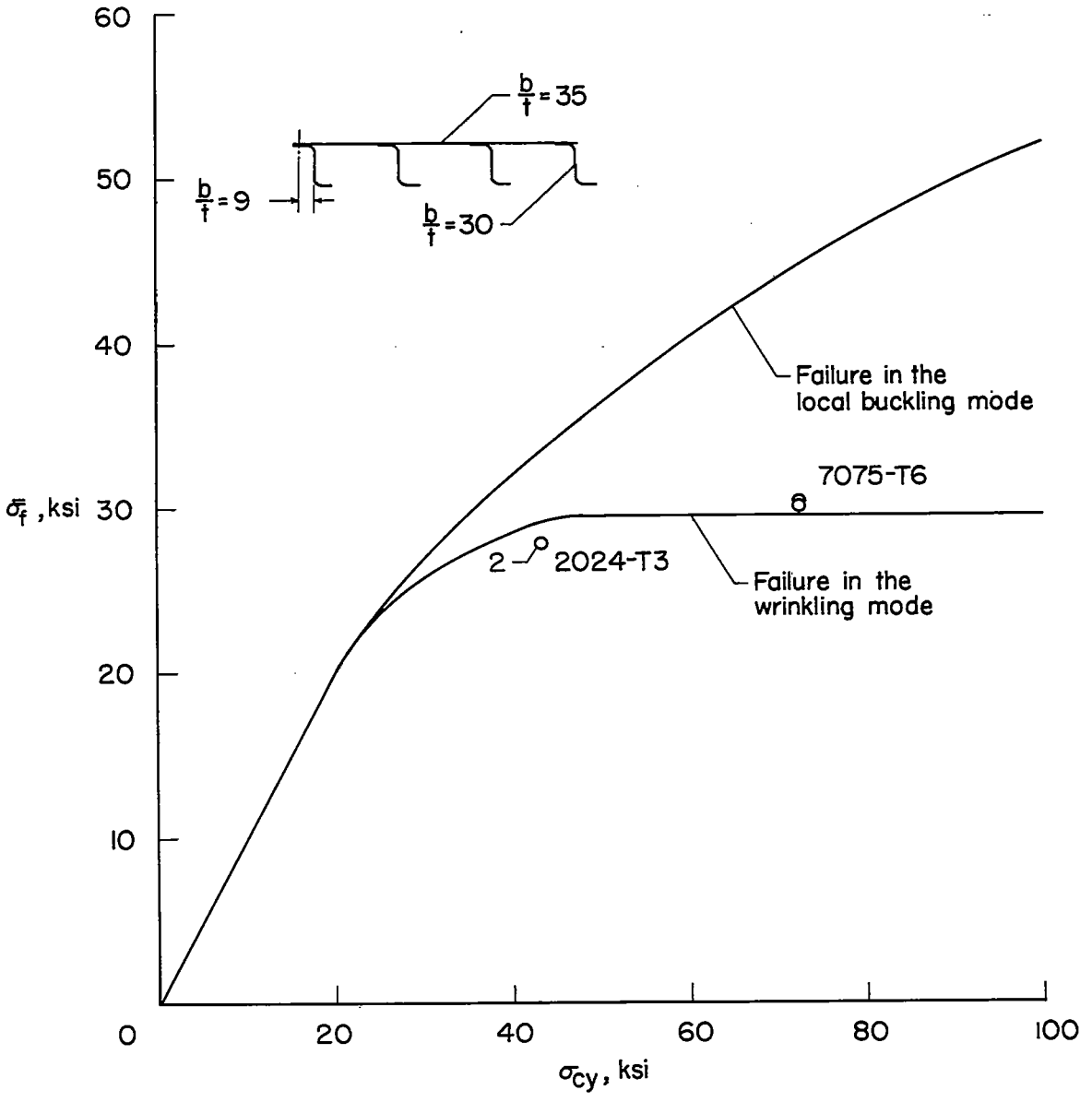

Figure 10.- Behavior of stiffened panel which fails in the wrinkling mode when tested in two different materials.

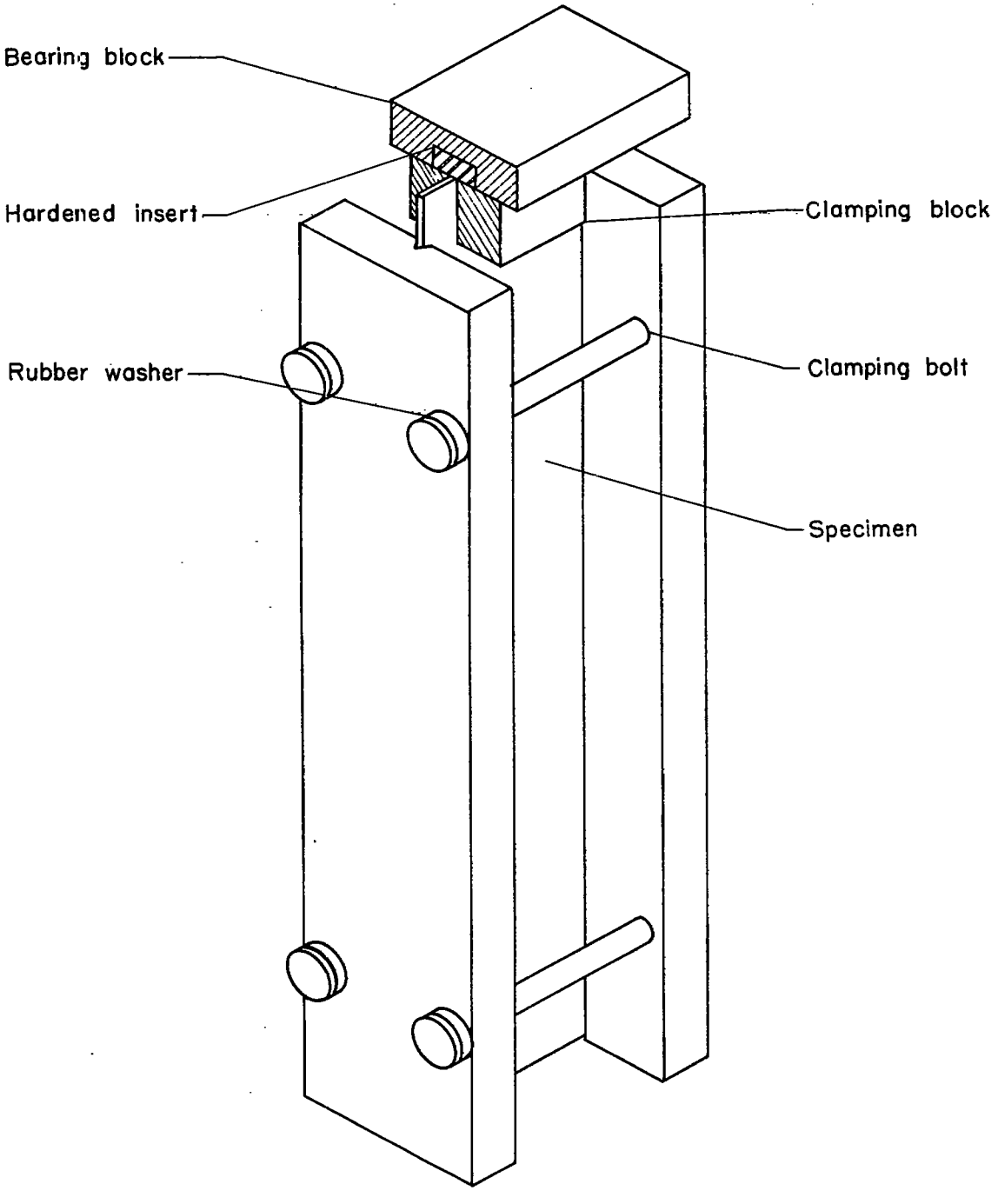

Figure 11.- V-groove edge fixture for plate compressive-strength test.

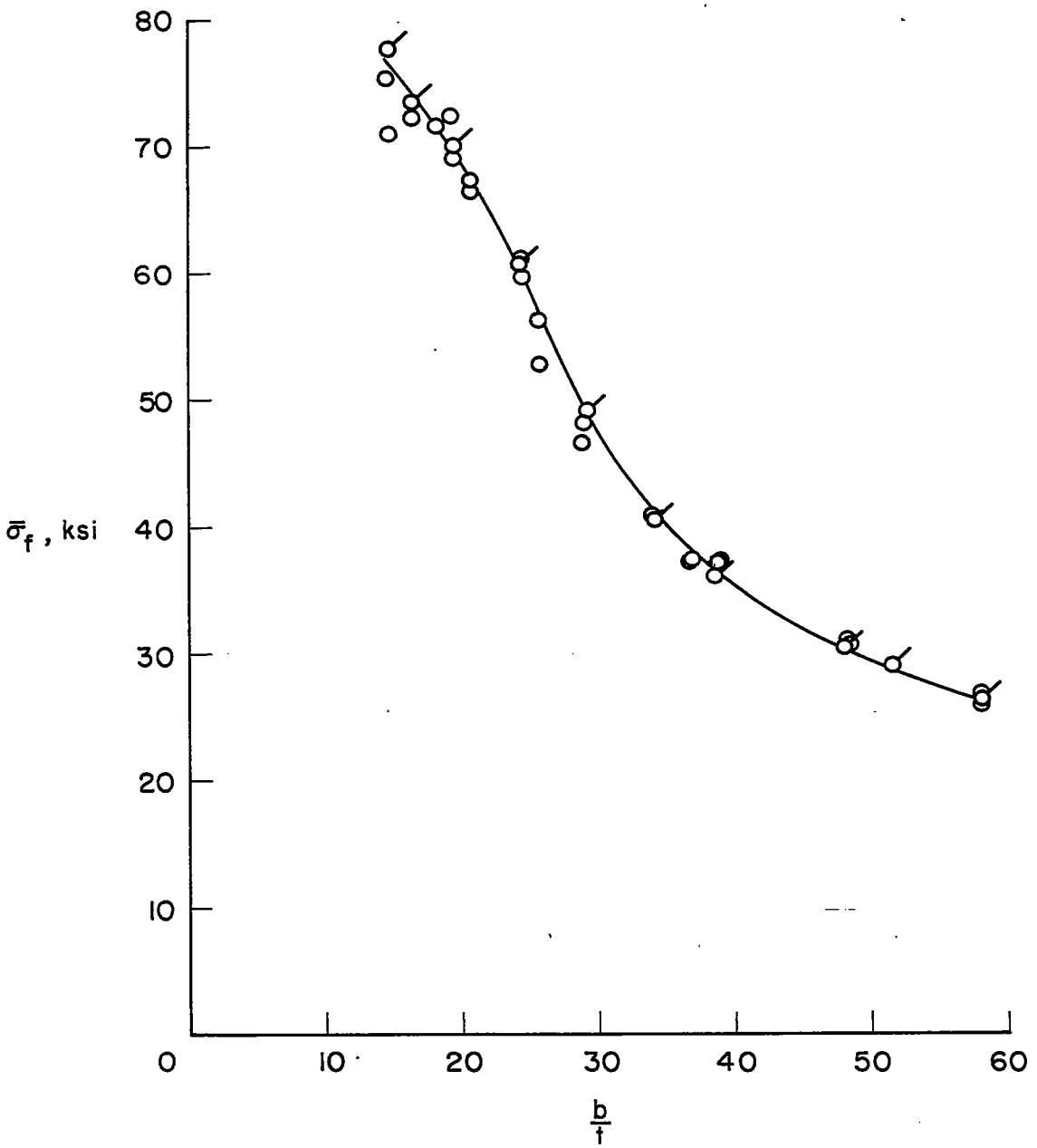

Figure 12.- Compressive-strength data obtained for plates of 7075-T6 aluminum alloy.

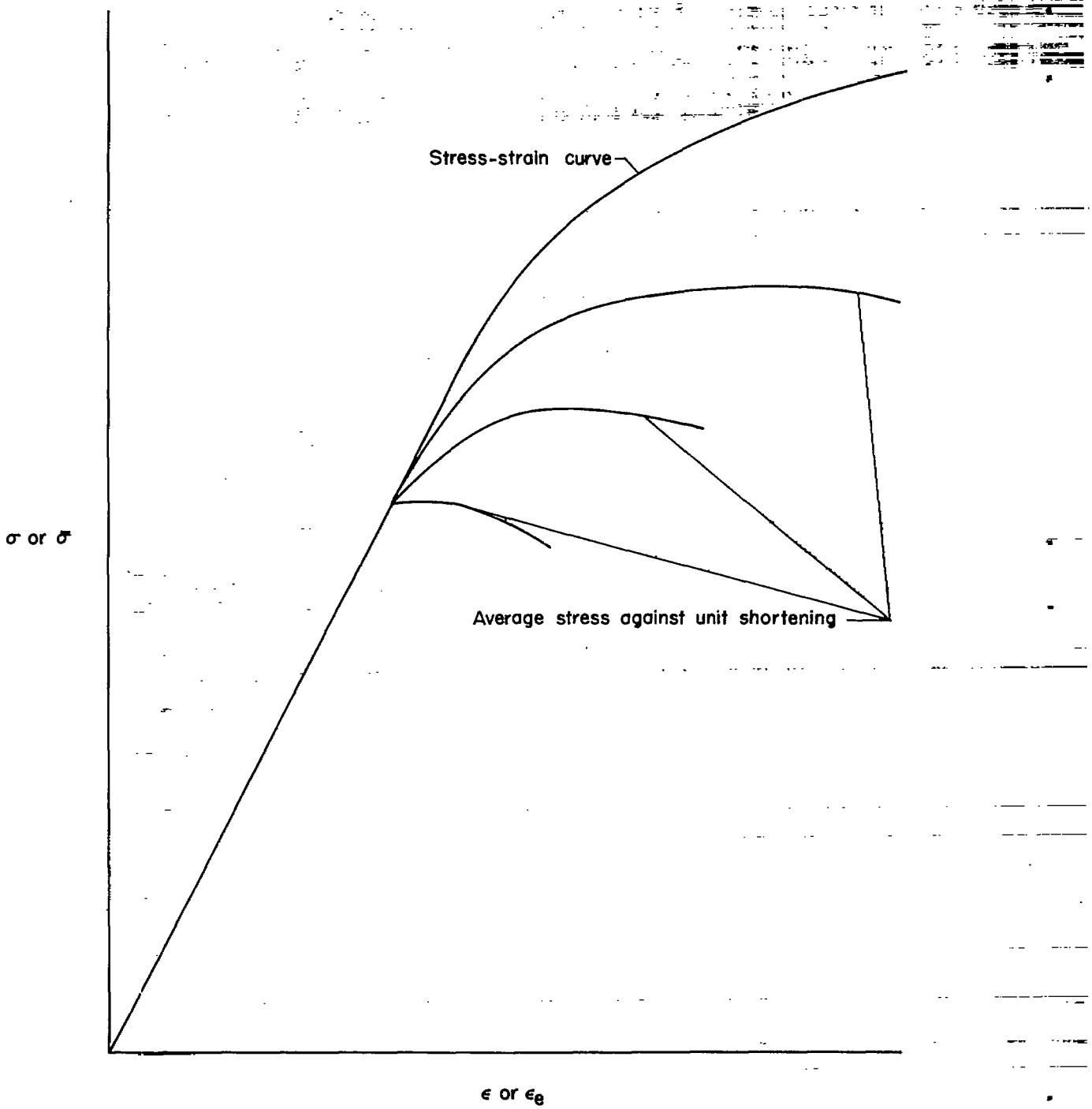

Figure 13.- Variation of average stress with unit shortening for three structures having same buckling stress.